

SEYFERT’S SEXTET: A SLOWLY DISSOLVING STEPHAN’S QUINTET?

A. DURBALA¹, A. DEL OLMO², M. S. YUN³, M. ROSADO⁴, J. W. SULENTIC¹, H. PLANA⁵, A. IOVINO⁶, J. PEREA²,
L. VERDES-MONTENEGRO², AND I. FUENTES-CARRERA⁷

¹ Department of Physics and Astronomy, University of Alabama, Box 870324, Tuscaloosa, AL 35487-0324, USA; adriana.durbala@ua.edu

² Instituto de Astrofísica de Andalucía, CSIC, Apdo. 3004, 18080 Granada, Spain

³ Department of Astronomy, University of Massachusetts, Amherst, MA 01003, USA

⁴ Instituto de Astronomía, Universidad Nacional Autónoma de México (UNAM), Apdo. Postal 70-264, 04510, México, D.F., Mexico

⁵ Laboratório de Astrofísica Teórica e Observacional, Universidade Estadual de Santa Cruz, Brazil

⁶ INAF—Osservatorio Astronomico di Brera, via Brera 28, 20121 Milano, Italy

⁷ GEPI, Observatoire de Paris, CNRS, Université Paris Diderot, Place Jules Janssen 92190, Meudon, France

Received 2007 May 30; accepted 2007 September 26; published 2007 December 7

ABSTRACT

We present a multiwavelength study of the highly evolved compact galaxy group known as Seyfert’s Sextet (HCG79: SS). We interpret SS as a 2–3 Gyr more evolved analog of Stephan’s Quintet (HCG92: SQ). We postulate that SS formed by sequential acquisition of 4–5 primarily late-type field galaxies. Four of the five galaxies show an early-type morphology which is likely the result of secular evolution driven by gas stripping. Stellar stripping has produced a massive/luminous halo and embedded galaxies that are overluminous for their size. These are interpreted as remnant bulges of the accreted spirals. H79d could be interpreted as the most recent intruder, being the only galaxy with an intact interstellar medium (ISM) and uncertain evidence for tidal perturbation. In addition to stripping activity we find evidence for past accretion events. H79b (NGC6027) shows a strong counter-rotating emission line component interpreted as an accreted dwarf spiral. H79a shows evidence for an infalling component of gas representing feedback or possible cross-fueling by H79d. The biggest challenge to this scenario involves the low gas fraction in the group. If SS formed from normal field spirals then much of the gas is missing. Finally, despite its advanced stage of evolution, we find no evidence for major mergers and infer that SS (and SQ) are telling us that such groups coalesce via slow dissolution.

Key words: galaxies: active – galaxies: elliptical and lenticular, cD – galaxies: interactions – galaxies: spiral

Online-only material: color figures

1. INTRODUCTION

Compact groups (CGs) are an intriguing component of large-scale structure (e.g. Hickson 1997). They can be described as contradictions in terms involving very high-density galaxy aggregates (typical projected separation ~ 30 – 40 kpc) found in some of the lowest galaxy density environments. In some ways they mimic a cluster-like environment (galaxy harassment/stripping/secular evolution). Early models (e.g. Mamon 1987; Barnes 1989) found them to be gravitationally unstable and therefore candidates for rapid collapse into “fossil” ellipticals. Unfortunately, very few fossil elliptical candidates have been found (Sulentic & Rabaça 1994; Zabludoff & Mulchaey 1998) except in denser and, especially, cluster environments. Very few CGs show signs of advanced merging (only $\sim 10\%$ contain a first ranked elliptical; Sulentic 1997). Dynamical models, taking into account massive dark matter (DM) haloes (Athanasoulas et al. 1997) or formation from a diffuse configuration (Aceves & Velázquez 2002), now suggest that such groups can survive for even a Hubble time.

One can study CGs both statistically and individually. Each approach has strengths and weaknesses. In either case, but especially the former, this requires a clear definition of the CG phenomenon. The most local samples (Iovino 2002; Hickson 1982, hereafter H1982) suggest that CGs can be defined as physically dense aggregates of 4–8 galaxies with separations on the order of a few component diameters. Quartets are by far the most common, while systems of 6–8 galaxies are rarely found. It is, of course, easier to identify numerical populations of such aggregates than to establish true physical density; however,

first attempts based on redshift concordance and evidence for interaction (Mendes de Oliveira & Hickson 1994) suggest that 60/100 of the aggregates in the Hickson compact groups (HCG) are *bona fide* compact groups (see, e.g., Table 2 in Sulentic 1997). It is assumed that triplets are dynamically distinct (inherently unstable) entities and should not be included in a compact group sample.

The above considerations suggest that CGs will be found in a wide range of evolutionary states (e.g. Ribeiro et al. 1998; Verdes-Montenegro et al. 2001) and that a detailed study of individual CGs might be best accomplished within the context of an assumed evolutionary stage. Relatively unstripped but interacting groups should be very young, while aggregates of early-type galaxies embedded in a common stellar halo should be highly evolved. All or most of the CGs that have formed in the local Universe may still exist as CGs. SQ and SS, two of the densest and best known groups, might be viewed as young/middle aged (few Gyr) and highly evolved (many Gyr) examples, respectively. We considered SQ earlier (Sulentic et al. 2001) and focus on SS in this paper. The best examples for detailed study involve those CGs with abundant multiwavelength data and SS certainly qualifies by that criterion. As one of the most evolved groups they provide a further motivation for detailed study.

Seyfert’s Sextet (HCG 79, VV 115) is probably the densest (most compact) galaxy aggregate in the local Universe (the systemic recession velocity is $v_R \sim 4400$ km s⁻¹, implying a distance $D \sim 60$ Mpc assuming $H_0 = 75$ km s⁻¹ Mpc⁻¹). It is also one of the most isolated systems (H1982; Sulentic 1987; Iovino 2002). In this paper we present new multiwavelength data

(optical, IR, and radio), including line and continuum imagery, Fabry–Pérot and slit spectroscopy. In addition to these datasets, the paper harvests previously published multiwavelength data for the group in an attempt to give a clear and coherent picture of the phenomena involved and the current evolutionary state. Much of our interpretation of SS will be within the context of our observations and ideas about SQ.

The paper is organized as follows: Section 2 gives basic observations and reduction information; Section 3 provides data analysis and presentation with minimal interpretation; and Section 4 inferences about the evolutionary history of SS using new and old observations and interpreted in the light of what we have learned about SQ. Within Section 2 and Section 3 we organize into subsections according to wavelength and/or date type (e.g., IR, radio, optical and imaging, spectroscopy, line, continuum). The discussion in Section 4 contains frequent citations of the relevant parts of Section 3 that support specific inferences.

2. NEW OBSERVATIONS OF SS

2.1. Broad-Band Optical Images

Optical properties (e.g. magnitudes, morphologies, geometry) of SS and its neighbors were derived from the Sloan Digital Sky Survey (SDSS) (Data Release 5: SDSS DR5; Adelman-McCarthy et al. 2007) images⁸. We downloaded *g*- and *r*-band flexible image transport system (FITS) format images of night sky (“corrected”) frames using the Catalog Archive Server⁹. The corrected frames are flat-field, bias, cosmic-ray, and pixel-defect corrected (Stoughton et al. 2002). Sky background fitting and subtraction were performed using the IRAF¹⁰ task IMSURFIT. The IRAF task ELLIPSE was used to derive surface brightness, deviation of isophotes from pure ellipses (Fourier coefficient *b*₄—fourth cosine coefficient of the Fourier expansion), position angle (PA) and ellipticity as functions of the semimajor axis. Positive and negative values of *b*₄ indicates disk and boxy isophotes, respectively. Photometric calibration¹¹ of SDSS images was accomplished using the *aa*, *kk*, and *airmass* coefficients (zeropoint, extinction coefficient, and airmass) from the TsField files. The surface brightness zeropoint was calculated as $2.5 \times \log(\text{exptime} \times 0.396^2) - 2.5 \times 0.4 \times (aa + kk \times \text{airmass})$, using the exposure time *exptime*

⁸ This study has made use of SDSS Data Release 5. Funding for the SDSS and SDSS-II has been provided by the Alfred P. Sloan Foundation, the Participating Institutions, the National Science Foundation, the U.S. Department of Energy, the National Aeronautics and Space Administration, the Japanese Monbukagakusho, the Max Planck Society, and the Higher Education Funding Council for England. The SDSS web site is <http://www.sdss.org/>. The SDSS is managed by the Astrophysical Research Consortium for the Participating Institutions. The Participating Institutions are the American Museum of Natural History, Astrophysical Institute Potsdam, University of Basel, University of Cambridge, Case Western Reserve University, University of Chicago, Drexel University, Fermilab, the Institute for Advanced Study, the Japan Participation Group, Johns Hopkins University, the Joint Institute for Nuclear Astrophysics, the Kavli Institute for Particle Astrophysics and Cosmology, the Korean Scientist Group, the Chinese Academy of Sciences (LAMOST), Los Alamos National Laboratory, the Max Planck Institute for Astronomy (MPIA), the Max Planck Institute for Astrophysics (MPA), New Mexico State University, Ohio State University, University of Pittsburgh, University of Portsmouth, Princeton University, the United States Naval Observatory, and the University of Washington.

⁹ <http://www.sdss.org/dr5/access/index.html>.

¹⁰ IRAF (Interactive Reduction and Analysis Facility) is distributed by the National Optical Astronomy Observatory, which is operated by the Association of Universities for Research in Astronomy, Inc., under cooperative agreement with the National Science Foundation: <http://iraf.noao.edu/>.

¹¹ <http://www.sdss.org/dr5/algorithms/fluxcal.html>.

Table 1
Photometric Observations

Observations	Telescope	Filter	N_{exp}	$T_{\text{exp}}(\text{s})$	Seeing
Broad-band	2.5 m NOT	<i>B</i>	4	1620	1.1
Images	2.5 m NOT	<i>R</i>	3	1330	0.9

of 53.907,456 s and pixel size of 0".396. Our magnitudes are conventional (“Pogson”) magnitudes.

We also obtained deep *B* and *R* filter CCD images of SS with the 2.5 m Nordic Optical Telescope (NOT) of the Observatorio del Roque de los Muchachos (La Palma), using the ALFOSC¹² spectrograph. The detector was a Loral/Lesser 2048 × 2048 pixels with a spatial scale of 0".19 which gives a field of view of 6'.5 × 6'.5. The broad-band images of SS were obtained on a single night of a three-night observing run with ALFOSC. A summary of the main characteristics of the images can be found in Table 1. Atmospheric conditions were photometric. Photometric calibration was accomplished with observations of ten different Landolt standard stars (from Landolt 1983, 1992 list) in the fields SA110 and SA92 obtained on the same night that we observed SS. Seven of these stars were observed four times during the night at four different airmasses and the other three stars were observed three different times at three different airmasses. We have in total 37 star flux measures during the night and could obtain with good reliability the extinction during that night allowing us to quantify the photometric conditions. The seeing was also good, as indicated in Table 1. Reduction and calibration of the images were carried out using standard techniques. Bias exposures were used to construct average bias images that were subtracted from the images of SS. Pixel-to-pixel variations were evaluated with a median-normalized sky flat-field in each filter. Flux calibration was carried out following the method developed by Young (1974). Standard star residuals in the final calibration were always smaller than 0.03 mag. The errors due to variations in the sky were smaller than 1%.

We downloaded seven *HST*/WFPC2 archival images¹³ (4-F555W and 3-F814W) of SS all with exposure times of 500 s. We used IRAF to reject cosmic rays and to combine images. The left panel of Figure 1 presents a 31 × 31 pixel high-pass median filtered image of the average of all seven images. Two contours are superimposed indicating the maximum extent of the luminous halo on *HST*/SDSS (solid) and NOT images (dotted). The inner contour corresponds to the maximum halo extent on a 51 × 51 pixels low-pass filtered *HST* average. The outer contour shows a circle best representing the halo extent on the NOT *B* – *R* image shown later in Figure 7. We also downloaded the flux-calibrated archival *HST*/WFPC2 F555W image of SS with total exposure time of 2000 s. The upper and lower right panels Figure 1 show 15 × 15 pixels low-pass median filtered images of H79b and c, respectively. Images were extracted and enlarged by a factor of 5.5.

2.2. Narrow-Band Optical–H α Images

H α interference filter images (0".533 pixels) were obtained with the Calar Alto (Centro Hispano Aleman) 2.2 m telescope

¹² The data presented here have been taken using ALFOSC, which is owned by the Instituto de Astrofísica de Andalucía (IAA) and operated at the Nordic Optical Telescope under agreement between IAA and the NBIfAFG of the Astronomical Observatory of Copenhagen.

¹³ This research is based on observations made with the NASA/ESA *Hubble Space Telescope* Wide Field Planetary Camera, obtained from the Data Archive at the Space Telescope Science Institute, which is operated by the Association of Universities for Research in Astronomy, Inc., under NASA contract NAS 5-26555. These observations are associated with program no. 8717.

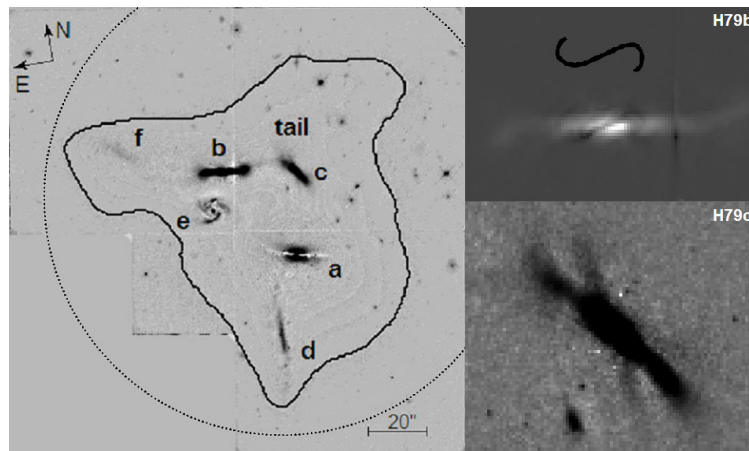


Figure 1. *HST*/WFPC2 images of SS. (left) a high-pass median filter image; (right) a low-pass median filter image (5.5× zoom in).

Table 2
Summary of Long-Slit Spectroscopic Observations at the NOT 2.5 m Telescope

Galaxy Slit direction	PA (deg)	Grism	N_{exp}	T_{exp} (s)	Disper. (Å/pixel)	Spectral range(Å)
H79b/H79b-c	81	GR4	3	1800	2.97	3027–9075
H79b/H79b-c	81	GR8	3	1800	1.24	5816–8339
H79c	35	GR4	3	1800	2.97	3027–9075
H79c	38	GR4	2	1200	2.97	3027–9075
H79c	38	GR8	2	1200	1.24	5816–8339
H79d	179	GR4	3	1800	2.97	3027–9075
H79d	179	GR8	4	3600	1.24	5816–8339
H79f	41	GR4	3	2700	2.97	3027–9075

in June 1997 (see also Xu et al. 1999). $H\alpha$ interference filter 667/8 centered at 6667 Å (FWHM = 76 Å) and Johnson R 641/158 centered at 6412 Å (FWHM = 157.5 Å) were used. Three different exposures were obtained with each filter (600s/exposure and 300s/exposure for 667/8 and Johnson R filters, respectively). The IRAF package was used for the $H\alpha$ reduction. The images were bias, flat field, cosmic ray, and sky corrected. Individual images were combined into average line and continuum images after centering, equalizing the psf and rescaling. $H\alpha + [N\text{ II}]\lambda\lambda 6548, 83$ equivalent widths were calculated following the relation from Iglesias-Páramo & Vílchez (1999):

$$EW(H\alpha + [N\text{ II}]) = \frac{C_\alpha}{C_{\text{cont}}} W_f,$$

where C_α is the number of galaxy counts in the net $H\alpha$ image, C_{cont} is the number of counts from the scaled continuum image, and W_f is the FWHM of the filter in Å.

2.3. Optical Spectroscopy (2D)

Long-slit spectra were obtained with ALFOSC at the NOT telescope with the same detector used for NOT images. Table 2 contains a summary of the long-slit observations with format as follows: Column 1, spectrum identification with the galaxy or the direction of the slit; Column 2, position angle; Column 3, grism used; Column 4, number of exposures in each slit; Column 5, total exposure time for each slit; Column 6, spectral resolution in Å/pixel; Column 7, spectral range.

The directions of the slits are marked in Figure 2. The spectra were reduced according to the usual techniques, including subtraction of a mean bias calculated for each night and division by a median flat field obtained for each configuration. Wavelength calibration was performed in a standard way using He–Ne lamps in each position. The rms of the bidimensional wavelength calibration was found to be of 0.06 Å for grism 8 and 0.4 Å for grism 4. In all cases several exposures were taken in order to increase the signal-to-noise ratio (S/N) and to remove cosmic rays. Spectra of the spectrophotometric standard stars BD+26 2606, HZ44, and BD+33 2642 were observed for flux calibration. Observations with grism 4 were performed in order to derive some general spectral characteristics of the galaxies. To obtain the kinematics of the galaxies we used the GR8 spectra with a spectral coverage from 5800 Å to 8300 Å and a spectral resolution of 1.24 Å/pixel. This setup includes the emission lines $H\alpha$, $[N\text{ II}]$, and $[S\text{ II}]$ together with the interstellar Na absorption.

In order to obtain redshifts and rotation curves we used the cross-correlation technique developed by Tonry & Davis (1979). For the emission line spectra we used as a templates brightest spatial section of galaxies H79b and H79d, together with a synthetic spectrum built from the rest frame wavelengths of the emission lines. In the case of the absorption line spectra, we used as a template a synthetic spectrum and exposures of three radial-velocity standard giant stars observed with the same setup.

2.4. $H\alpha$ Fabry–Pérot Spectroscopy (3D)

Scanning Fabry–Pérot (FP) $H\alpha$ interferometry was carried out during the nights of 2000 March 7 and 8, and 2001 March 24 using the FP interferometer PUMA (Rosado et al. 1995) attached to the $f/7.9$ Ritchey–Chretien focus of the 2.1 m telescope at the Observatorio Astronómico Nacional (San Pedro Martir—SPM, Baja California). PUMA involves a scanning FP interferometer, a focal reducer with an $f/3.95$ camera, a filter wheel, a calibration system, and a Site 1024×1024 CCD detector. The CCD readout was binned 2×2 resulting in a pixel size of $1''.16$ with a 10×10 arcmin field of view (FOV). The FP has an interference order of 330 at 6563 Å. The free spectral range of 934 km s^{−1} was scanned in 48 steps with a sampling resolution of 19 km s^{−1}.

We obtained five data cubes at 6658 Å, each with an exposure time of 120 s per channel (implying a total exposure time of

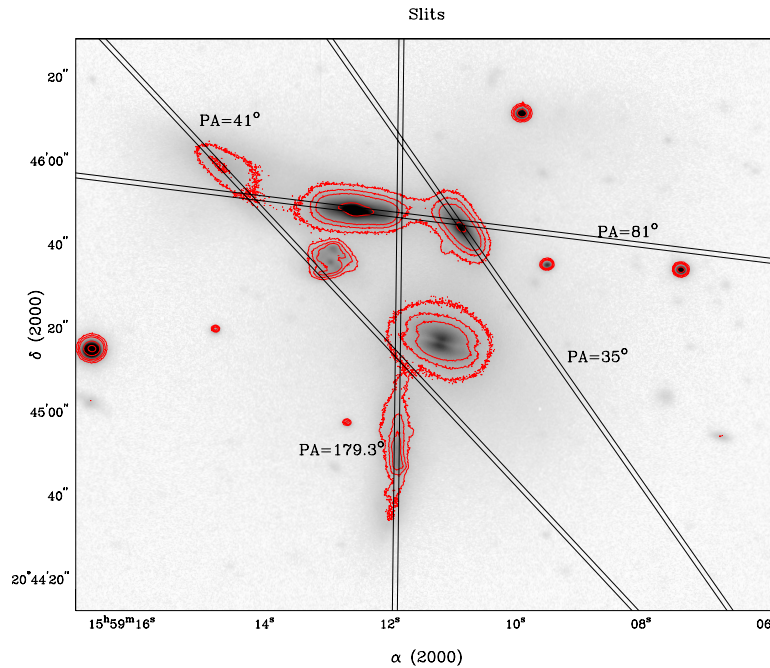


Figure 2. SS: the direction of the slits for the long-slit spectra obtained with ALFOSC at the NOT telescope. (A color version of this figure is available in the online journal)

Table 3
Journal of Fabry–Pérot Observations

Observations	Telescope	CFHT 3.6m	OAN 2.1m
	Equipment	MOS/FP @ Cassegrain	PUMA @ Cassegrain
	Date	1996 August 25	2001 March 24
	Seeing	0.6''	~1.2''
Calibration	Comparison light	λ 6598.95 Å	λ 6598.95 Å
Fabry–Pérot	Interference order	1162 @ 6562.78 Å	330 @ 6562.78 Å
	Free spectral range at H α	265 km s ⁻¹	934 km s ⁻¹
	Finesse at H α	12	24
	Spectral resolution at H α	13672 ^a	7457 ^a
Sampling	Number of scanning steps	24	48
	Sampling step	0.24 Å (11 km s ⁻¹)	0.44 Å (19 km s ⁻¹)
	Total field	220'' × 220'' (256 × 256 pixel ²)	604'' × 604'' (512 × 512 pixel ²)
	Pixel size (binned)	0.86''	1.16''
Detector		STIS 2 CCD	Site CCD
Exposure time		180s/ch	120s/ch
Interference filter	Central wavelength	6665 Å	6650 Å
	FWHM	19 Å	30 Å
	Transmission	0.55 @ 4500 km s ⁻¹	0.70 @ 4500 km s ⁻¹

Note. ^a For a S/N of 5 at the sample step.

96 min per data cube), during our observing runs. We selected the best data cube (the data cube with best seeing and transparency conditions) in order to do our analysis. The best data cube was from 2001. A log of FP observations is presented in Table 3.

The calibration of the data cubes was carried out by obtaining, under the same observing conditions, calibration cubes using the line at λ 6598.95 Å of a diffuse neon lamp. The calibration cubes were obtained before and after SS observations in order to check for possible flexures of the instrument.

Reduction of the data cubes was carried out using the CIGALE/ADHOCw software (Boulesteix 1993; Le Coarer et al. 1993). The data reduction procedure has been extensively described in Amram et al. (1991) and Fuentes-Carrera et al.

(2004). The accuracy of the zero point for the wavelength calibration is a fraction of a channel width (≤ 3 km s⁻¹) over the whole field. OH night-sky lines passing through the filter were subtracted by determining the emission in the field outside SS (Laval et al. 1987).

From PUMA observations we can extract, in addition to the velocity cubes, velocity profiles and the 2D velocity fields of the objects as well as purely monochromatic and continuum images obtained by integrating the intensities of the radial velocity profiles, pixel per pixel, up or down to a certain value of the velocity peak, respectively.

The Canada–France–Hawaii Telescope (CFHT) data reduction procedure has been extensively described in Amram et al. (1992) and references therein. A summary of the FP observations can be found in Table 3.

Wavelength calibration was obtained by scanning the narrow Ne 6599 Å line under the same conditions as the observations. Velocities measured relative to the systemic velocity are very accurate, with an error of a fraction of a channel width ($<3 \text{ km s}^{-1}$) over the whole field.

Subtraction of bias, flat fielding of the data, and cosmic-ray removal have been performed for each image of the data cube for the CFHT observations. To minimize seeing variation, each scan image was smoothed with a Gaussian function of FWHM equal to the worst-seeing data of the data cube. Transparency and sky foreground fluctuations have also been corrected using field star fluxes and galaxy-free windows for the observations.

The signal measured along the scanning sequence was separated into two parts: (1) an almost constant level produced by the continuum light in a narrow passband around H α (continuum map), and (2) a varying part produced by the H α line (H α -integrated flux map). The continuum level was taken to be the mean of the three faintest channels, to avoid channel noise effects. The H α integrated flux map was obtained by integrating the monochromatic profile in each pixel. The velocity sampling was 11 km s^{-1} at CFHT. Profiles were spatially binned to 3×3 or 5×5 pixels in the outer parts, in order to increase the S/N. Strong OH night sky lines passing through the filters were subtracted by determining the level of emission from extended regions away from the galaxies (Laval et al. 1987).

2.5. Mid-Infrared

Mid-infrared (MIR) observations for SS were obtained in the raster imaging mode (AOT:ISOCAM01) with the mid-infrared camera ISOCAM (Cesarsky et al. 1996) on board the *Infrared Space Observatory (ISO)* (Kessler et al. 1996).

We observed our group using the filter LW10, centered at $11.5 \mu\text{m}$, and the configuration with a pixel field-of-view (PFOV) = $6''$ for the 32×32 infrared array. We adopted a raster mode 2×2 , with a raster step of $9''$, for a total exposure time of 450 s on target (each single exposure had 10 s integration).

The data were reduced using the software CIA (CAM Interactive Analysis, v. 3) and included standard steps such as dark subtraction, removal of cosmic rays events (deglitching), correction for the transient of the detector (stabilization), averaging the frames at each raster position and flat-field correction, and finally combining the frames at each position into one mosaic image taking into account the instrument distortions (projecting; for a detailed description of these steps, see Siebenmorgen et al. 1996).

Figure 15 shows the isophotal contours of the $12 \mu\text{m}$ image overlapped on a Palomar Digital Sky Survey (DPOSS) image of the same group.

In ISOCAM images a major source of photometric error is due to variation of the sky background, correction for the transient (memory) effect, and undersampling of the objects. In our case the near-blending of galaxies H79b and e is a further source of error. A conservative estimate for the accuracy of our measured fluxes is $\sim 25\%$ (see also Siebenmorgen et al. 1996; Biviano 1998).

2.6. Radio Line and Continuum

Observations of SS using the Very Large Array (VLA¹⁴) were conducted in its 3 km (C) and 1 km (D) configuration

on 1997 August 2 and 1998 February 6, respectively, using all 27 telescopes (the VLA programs were AY85 and AY86). Shortest baselines at the shadowing limit of 25 m are present, and structures as large as $15'$ in size should be visible in each channel maps. The spectrometer was configured in the dual polarization 2IF mode to have 64 spectral channels at a frequency resolution of 48.8 kHz ($\sim 10.5 \text{ km s}^{-1}$) to cover a total bandwidth of 3.125 MHz ($\sim 660 \text{ km s}^{-1}$). All of the data were calibrated following the standard VLA calibration procedure in AIPS and imaged using IMAGR. The absolute uncertainty in the resulting flux scaling was about 15%, and this is the formal uncertainty we quote for all physical parameters derived from the flux density.

The synthesized beam produced using a robust weight of $R = 1$ was $27''.0 \times 16''.4$. The resulting spectral-line maps had an rms noise level of $0.5 \text{ mJy beam}^{-1}$. The 3σ H I flux limit in each map was about $0.016 \text{ Jy km s}^{-1}$, corresponding to an H I column density limit of $4 \times 10^{19} \text{ atoms cm}^{-2}$. At the adopted distance of the compact group (60 Mpc), the corresponding mass detection limit was $1.4 \times 10^7 M_{\odot}$.¹⁵

A line-free continuum image constructed by averaging the 14 line-free channels is shown in Figure 16. This continuum image had an effective bandwidth of 1.37 MHz centered on an effective frequency of 1399 MHz. The rms noise level achieved in Figure 16 was $0.20 \text{ mJy beam}^{-1}$.

In addition, we also produced a higher resolution 1.4 GHz continuum image of SS using the data from the archive. The *B*-configuration snapshot image with $\sim 5''$ resolution was obtained in the continuum mode with a total bandwidth of 200 MHz, and the rms noise in the image was $\sim 0.06 \text{ mJy beam}^{-1}$.

3. DATA ANALYSIS

3.1. Broad Band Optical

3.1.1. SS Environment

One of the characteristics of the best known local examples of CGs (H1982; Iovino 2002) involves the low galaxy surface density environments in which they are found. Since they are usually selected with an isolation criterion, it is not surprising that they are at least locally isolated but they are often so compact that this does not necessarily mean very much in the context of loose group scales. Attempts have been made to estimate the galaxy surface density near H1982 groups over a larger area/volume (Sulentic 1987; Rood & Williams 1989) and a redshift survey has also identified accordant redshift neighbors around 17 Hickson groups (de Carvalho et al. 1997). Many were found to be quite isolated even on Mpc scales where they are often found on the periphery of nearby superclusters in stark contrast to their implied space densities that can exceed those of cluster cores. SS is arguably the most compact group in the local Universe showing the largest surface density enhancement of any Hickson group. A little reconnaissance usually allows one to identify the component of the large-scale structure with which a CG is associated. SS can be assigned to group LGG403 (Garcia 1993; Rood & Struble 1994) whose identified members span several Mpc. NED¹⁶ reveals only one accordant

¹⁵ The atomic gas mass has been calculated as $M_{\text{HI}} = 2.36 \times 10^5 D_{\text{Mpc}}^2 \int S_V dV$, where $S_V dV$ is in Jy km s^{-1} .

¹⁶ This research has made use of the NASA/IPAC Extragalactic Database (NED) which is operated by the Jet Propulsion Laboratory, California Institute of Technology, under contract with the National Aeronautics and Space Administration.

¹⁴ The VLA is operated by the National Radio Astronomy Observatory, which is a facility of the National Science Foundation, operated under cooperative agreement by Associated Universities, Inc.

Table 4
Properties of Members of SS and Neighbor Galaxies

Galaxy	R.A. (J2000)	Decl. (J2000)	v_r	Morphological	Distance from SS	
	(hh mm ss.s)	(+dd mm ss.s)	(km s ⁻¹)	Type	(')	(kpc)
HCG79 a	15 59 11.1	+20 45 16.5	4292 ^a	E3		
HCG79 b	15 59 12.5	+20 45 48.1	4446 ^a	S0		
HCG79 c	15 59 10.8	+20 45 43.4	4146 ^a	S0		
HCG79 d	15 59 11.8	+20 44 48.7	4503 ^a	Sd		
HCG79 e	15 59 12.9	+20 45 35.4	19809 ^a	Sc		
HCG79 f	15 59 14.9	+20 45 57.3	4095 ^b	SO?		
UGC 10127	16 00 24.0	+20 50 56.9	4823 ^b	Sb	17.7	309
CGCG 137-004	15 56 33.7	+21 17 21.0	4367 ^c	S0	48.7	850
UGC 10117	15 59 23.9	+21 36 12.7	5375 ^d	Sab	50.8	887
CGCG 137-019	16 02 30.5	+21 07 14.3	4555 ^d	E	51.2	894
NGC 6032	16 03 01.1	+20 57 21.5	4282 ^c	SBb	54.2	958
CGCG 108-053	16 01 07.1	+19 26 54.6	4347 ^b	S0	83.1	1450
NGC 6052 NED01	16 05 12.9	+20 32 32.5	4500 ^e	Sc	85.4	1490
NGC 6052 NED02	16 05 13.2	+20 32 32.7	4541 ^e	Sc	85.5	1492
NGC 6008B	15 53 08.3	+21 04 28.5	5119 ^c	E/SO	87.0	1518
NGC 6028	16 01 29.0	+19 21 35.6	4475 ^b	(R)Sa	89.9	1569
NGC 6008	15 52 56.0	+21 06 01.8	4869 ^b	SBb	90.1	1572
UGC 10197	16 06 04.4	+20 48 05.4	4771 ^c	Sd	96.5	1684
UGC 10198	16 06 05.9	+20 47 03.3	4624 ^f	Sdm	96.8	1690
CGCG 137-037	16 05 59.5	+21 21 37.2	4428 ^c	Sa?	101.7	1775
NGC 6020	15 57 08.1	+22 24 16.3	4307 ^g	E	102.9	1796
NGC 6060	16 05 52.0	+21 29 05.9	4439 ^b	SBc	103.0	1798
CGCG 108-085	16 03 26.6	+19 09 44.0	4684 ^h	Im	112.9	1970

References. ^a Hickson et al. (1992); ^b RC3; ^c Falco et al. (1999); ^d Beers et al. (1995); ^e Tarengi et al. (1994); ^f Freudling (1995); ^g Müller et al. (1999); ^h Barmby & Huchra (1998).

redshift (3400–5400 km s⁻¹) neighbor (UGC10127) within 30' (~0.5 Mpc) radius. Only four additional accordant (within ±1000 km s⁻¹) galaxies are found within 60' (CGCG137-004, UGC 10117, CGCG137-019, NGC6032). This radius corresponds to crossing time $t_c \sim 5$ Gyr assuming a random velocity on the plane of sky of 200 km s⁻¹.

Table 4 provides a census of the 17 known accordant redshift neighbors within 2 Mpc (an Abell radius) of SS and within 1000 km s⁻¹ of the mean group recession velocity. This census is based upon SDSS images of the field and includes all galaxies brighter than g magnitude of the faintest member of SS (H79d with $g \sim 15.5$; redshift implied luminosity similar to the Large Magellanic Cloud (LMC)). Redshifts were taken from NED because the SDSS does not provide spectroscopy for this field. The g -band survey also found 12 galaxies beyond 5500 km s⁻¹ (many near 10–11,000 km s⁻¹ associated with the Hercules Cluster), one galaxy near 2000 km s⁻¹ and three without redshift measures. An equivalent r -band census to $r = 15.8$ (r -band magnitude of H79d) yields many more galaxies (without redshifts) but visual inspection suggests that all/most of these are likely to be much more distant. We adopted the g -band census because (1) it shows higher redshift completeness, (2) we wanted to minimize background contamination, and (3) we regard late-type field galaxies as the principal source of infalling intruders as suggested by NGC7318b in SQ and H79d in SS. The census yields a surface density of 1.3 galaxies Mpc⁻², or 1.6 galaxies Mpc⁻² if all three bright neighbors with unmeasured redshift show accordant measures. Some recent surface density estimates range from ~1 Mpc⁻² for the sparsest environments up to ~6 Mpc⁻² in the poorer cluster cores (Goto et al. 2003a). SS shows a surface density of ~7–8000 galaxies Mpc⁻² and a surface density enhancement of ~5–6000 in agreement with Sulentic (1987). SS shows the highest density enhancement of

any compact group in the local Universe and one of the lowest galaxy surface densities in its Mpc-scale environment.

3.1.2. SS Component/Neighbor Morphologies and Geometries

SS involves four or five accordant redshift (H79abcdf) galaxies plus one discordant redshift galaxy (H79e). H79f on the NE edge of the group can be described either as a tidal tail or as the remnants of a tidally stripped galaxy. The mean separation between the galaxies is about 7.2 kpc and the mean velocity dispersion $\sigma_V = 121$ km s⁻¹ (hereafter D2005)(Da Rocha & Mendes de Oliveira 2005). Figure 1 identifies specific components of the group following designations in Hickson (1982; 1993a) with the addition of H79f.

Table 4 gives estimated Hubble types for assumed members of SS as well as all neighbors within a radius of ~2 Mpc. Positions and recession velocities are given for all galaxies along with projected separations in arcmin and kpc for the neighbors. SS members show unusual and sometimes ambiguous structure. Figures 3 and 4 present the most interesting standard geometric profiles for the two brightest member galaxies (H79ab). We derived these measures from r -band SDSS images. Results for the g band were very similar. Several sets of geometric profiles and derived parameters have already been given for galaxies in SS: Hickson et al. (1989a), hereafter H1989a; Rubin et al. (1991), hereafter R1991; Bettoni & Fasano (1993), hereafter B1993; Nishiura et al. (2000a), hereafter N2000a. A serious problem with deriving standard parameters for SS components involves the fact that they are embedded in a luminous halo. For example, the r -band surface brightness of the last concentric isophotes in H79abc are 21.7, 21.0, and 21.2 mag arcsec⁻², respectively.

The three brightest members (H79abc) all show early-type morphologies in the simple sense that they are axially symmetric

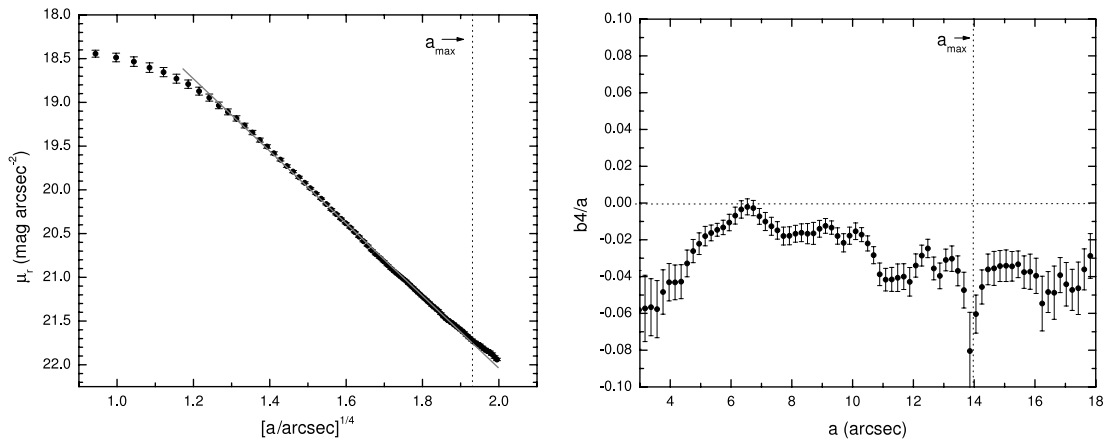


Figure 3. H79a: (left) elliptically averaged surface brightness profile in the r band; (right) b_4 coefficient profile. The dotted horizontal line corresponds to a fourth cosine Fourier coefficient of 0 (perfect ellipse). We truncated the profile from 3 arcsec because of the dust lane.

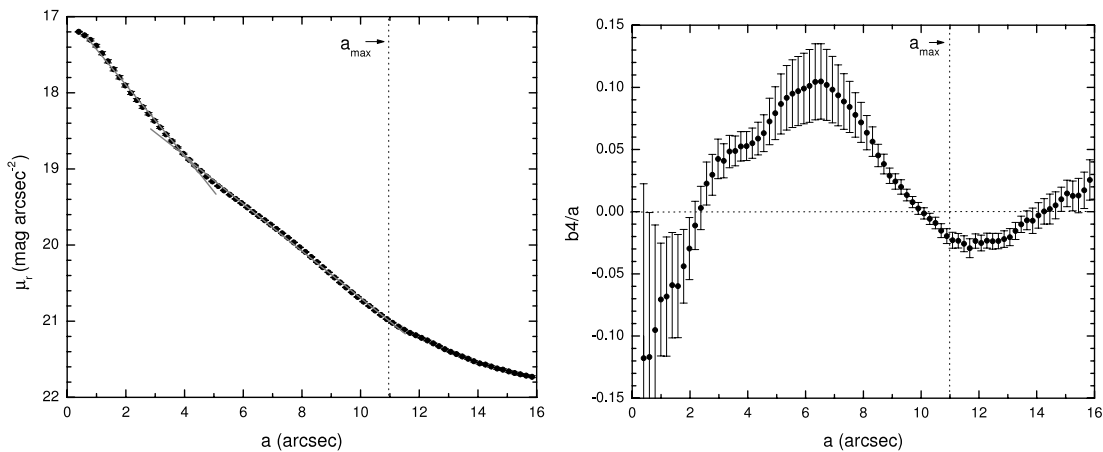


Figure 4. H79b: (left) elliptically averaged surface brightness profile in the r band; (right) b_4 coefficient profile. The dotted horizontal line corresponds to a fourth cosine Fourier coefficient of 0 (perfect ellipse).

with no obvious spiral arms or visible emission regions. H79a (NGC6027a) shows a very smooth light distribution and an ellipticity consistent with Hubble type E3-4 although it has been classified E0, S0, and Sa in the past. It is bisected by a prominent dust lane, adding to the confusion in assigning a type and in determining the position of the nucleus. The relaxed appearance (i.e. flatness) of the dust lane forces us to consider the possibility that H79a might be an edge-on S0 with a weak stellar disk component. The alternative interpretations are that the dust lane (1) hints that H79a was originally a spiral galaxy or (2) is the relaxed signature of a past accretion event. “Relaxed” is perhaps an overstatement because the dust lane shows a pronounced bend (see Figure 1) in the direction towards the center of the group. Figure 3 shows azimuthally averaged surface brightness and b_4 profiles for this galaxy derived with fixed position angle (68°) and ellipticity ($\epsilon = 0.36$). In the figures a_{\max} indicates the semimajor axis of the last concentric isophote. Isophotal boxiness is observed in the center and is probably induced by the dust lane (see also B1993). No surface photometric study of this galaxy has revealed a stellar disk component that might be a counterpart to the dust disk.

The unusual shape and internal structure of H79b revealed by HST images (Figure 1) do not lend themselves to a standard geometric analysis. Figure 4 shows evidence for two disk components (centered at $\approx 2\text{--}3''$ and $5\text{--}8''$) in both surface

brightness and b_4 parameter. Seeing in the SDSS r -band image is ~ 2.5 pixels corresponding to $\sim 1''$. The above-mentioned WFPC2 images show signs of highly inclined internal (spiral?) structure (see Figure 1 (upper right) where a tightly wrapped spiral dust lane is seen). Earlier WFPC1 images revealed the presence of a twisted dust lane oriented approximately diagonally across the galaxy (Sulentic et al. 1994). The axial ratios of H79b and c suggest that both are highly inclined to our line of sight. The surface brightness and b_4 profiles for H79c also indicate considerable complexity. The WFPC2 images suggest that the tidal tail extending to the NW originates near this galaxy. It crosses the disk at an angle of about 20° forming an apparent “X” structure (see Figure 1 (lower right)).

H79d is the only member that shows a late-type (spiral) morphology with numerous condensations resembling H II regions detected on many images but most dramatically with WFPC2. It is highly inclined with an axial ratio of 0.18 suggesting an inclination of 80° . H79d appears to be projected on H79a because a few dusty condensations can be seen in silhouette against the halo light of that galaxy on the WFPC2 images (Palma et al. 2002). Some published studies suggest a link between galaxies H79ad (R1991; Plana et al. 2002).

H79e shows a much higher redshift and is assumed to be a near-face-on high-luminosity Scl spiral at approximately 4.5 times greater distance. H79f lies to the NE of H79b and is

Table 5
SS Sizes

HCG79	Our data		Our data		H1989a	B1993	RC3	N2000a
	D_g^a (")	D_g^a (kpc)	D_r^a (")	D_r^a (kpc)	D_R^b (kpc)	D_R^c (kpc)	D_B^d (kpc)	D_{VR}^e (kpc)
a	25	7.4	28	8.1	14.7	6.7	11.8	4.6
b	22	6.5	22	6.5	13.6	3.3	7.6	2.0
c	18	5.3	18	5.3	10.4	6.3	6.9	1.5
d	32	9.4	26	7.6	4.7	...	15.2	4.7
f	17	5.1	17	5.1	13.9	3.7

Notes.

^a D_g and D_r are equal to $2 a_{\max}$, where a_{\max} is the semimajor axis of the last concentric isophote in the g and r bands, respectively.

^b Diameter of $\mu_R = 24$ R -mag arcsec⁻² isophote, where $D_R = \sqrt{A_R/\pi}$ and A_R is the area of the isophote.

^c $D_R = 2 r_e$, where r_e is the effective radius in the R band.

^d Diameter of $\mu_B = 25$ B -mag arcsec⁻² isophote.

^e $D_{VR} = 2 r_e$ for galaxies a and c, where r_e is the effective radius in the VR band; $D_{VR} = 2 h$ for galaxies b, d and f, where h is the disk scale length in the VR band.

either a tidal filament or another early-type member. It was not included as a member by Hickson (1982, 1993a) yet the RC3 catalog (hereafter RC3)(de Vaucouleurs et al. 1991) lists it as a galaxy with designation NGC6027e. The surface brightness profile for this galaxy follows an exponential law. The position angle and ellipticity profiles in the outer part of H79f are constant ($\sim 50^\circ$ and ~ 0.57 , respectively). The surface brightness of the last concentric isophote in H79f is 21.6 mag arcsec⁻² in the r band and 22.3 mag arcsec⁻² in the g band. The central concentration and elliptical isophotes argue that it is a member galaxy; however, in this interpretation it has likely been heavily stripped given the weakness of the central concentration for an apparently early-type morphology (lacking any signs of gas or dust).

Perhaps more unusual than their internal peculiarities are the small measured sizes of all members of SS. Table 5 presents different estimates for the sizes of the galaxies in SS. We compare our SDSS based measurements with four previous studies (H1989a, B1993, RC3, and N2000a). We find a large scatter among the measures consistent with the difficult task of extracting discrete diameters from galaxies embedded in a luminous halo. Measured diameters exceed 10 kpc only if one attempts to apply a standard model of the galaxy that extends beyond the last concentric isophote. We used SDSS g - and r -band images to determine the last concentric major/minor axis isophotes in each galaxy. We think that attempts to measure standard diameters (e.g. 25 mag arcsec⁻²) have little or no meaning in the context of individual galaxy properties since this level is three magnitudes below the surface-brightness level of the last concentric isophote. The luminous halo of SS likely contains a significant fraction of the stellar mass of galaxies H79abc and especially H79f. Attempts at model-based (e.g. exponential and $r^{1/4}$) galaxy subtraction of H79abcdf suggest that the halo is not a product of isophotal overlap (N2000a Sulentic & Lorre 1983). Galaxy H79d is the only component of SS that shows little sign of tidal stripping and appears to be a recently arrived low-luminosity late-type spiral.

The shape and extent of the luminous halo in SS is indicated by two contours in Figure 1. The inner very irregular contour shows the extent of the halo on HST and SDSS images. In the latter case this corresponds to 24.7 and 24.2 mag arcsec⁻² in the g and r bands, respectively. The outer more symmetric contour shows the circle best fitting the halo extent on more sensitive NOT B -band images (see also Figure 7) and corresponds to

27 mag arcsec⁻². The radius of the outer circle is 1.3 arcmin (~ 23 kpc). The SDSS sky levels at that radius are 26.4 and 26.2 arcsec⁻² for the g and r bands, respectively.

Seventeen accordant redshift neighbors brighter than $g = 15.5$ lie within ± 1000 km s⁻¹ and $r = 2 Mpc$ of SS. Table 4 lists the assigned Hubble types for the galaxies with 75–80% of SS members (3/4 or 4/5 depending on whether H79f is considered) and 30–40% of neighbors showing early-type (E/S0 or E/S0/Sa) morphologies. Recent morphological re-evaluation of a sample of about 1000 very isolated field galaxies (Sulentic et al. 2006) leads us to predict a $\sim 14\%$ early-type fraction in SS and in its neighborhood. The SS environment shows a 2–3 times higher early-type fraction, so this prediction is likely too low. A recent quantification of the morphology–density relation (Goto et al. 2003a) finds 16% E plus 30% S0 for environments with surface density similar to the SS neighborhood, suggesting that the observed early-type galaxies are overrepresented in SS if we accept H79abc, and possibly f, as *bona fide* E/S0 galaxies.

Table 6 provides g -band major axis diameters at the 25 mag arcsec⁻² isophote derived from the SDSS images for 13 accordant redshift neighbors. Comparison of these diameters with those for SS components leads to the conclusion that the galaxies in SS are 3–4 times smaller. A similar conclusion was found by Williams et al. (1991) where they noted that the individual galaxies in SS are on average one third the size of a typical normal galaxy. We estimated the diameters of neighboring S0-Sb galaxies truncated to the same surface brightness level as the last concentric isophotes in H79abc. We find neighbor diameters in the range 4–7 kpc at $\mu_g = 21.5$ mag arcsec⁻² and 4–12 kpc at $\mu_g = 21.8$ mag arcsec⁻² compared to 5–8 kpc for H79abc at their last concentric isophotes. The SS members are therefore more similar in size to the bulge components of neighboring spiral galaxies. The galaxies in SS are either (a) intrinsically dwarf or (b) normal galaxies that have undergone severe tidal stripping. The angular size of the entire group is ~ 1.3 arcmin (H1982) ~ 23 kpc which is comparable to the size of some of the neighboring disk galaxies. The massive common halo in SS implies significant stripping and disfavors the hypothesis that most SS members are intrinsically dwarf galaxies.

3.1.3 SS Component and Neighbor Luminosities

Table 7 presents apparent magnitudes for members of SS in different filters. We compare our g - and r -band SDSS-

Table 6
Neighbor Sizes, Magnitudes, and Luminosities

Galaxy	D_{25g} (kpc)	$D_{21.5g}$ (kpc)	$D_{21.8g}$ (kpc)	g_{TC}	M_g	r_{TC}	M_r	L_{rT} ($10^{10}L_{\odot}$)	L_{rB} (10^9L_{\odot})
(1)	(2)	(3)	(4)	(5)	(6)	(7)	(8)	(9)	(10)
UGC 10127	40.6	4.5	12.4	13.0	-21.0	12.3	-21.7	3.9	11.3
CGCG 137-004	20.7	5.1	5.9	13.7	-20.1	13.0	-20.8	1.7	11.6
UGC 10117	28.0	6.5	7.7	13.5	-20.8	12.8	-21.4	3.0	11.7
CGCG 137-019	22.1	13.7	-20.2	13.0	-20.9	1.9	...
NGC 6032	27.4	2.7	4.4	12.9	-20.8	12.3	-21.4	3.0	8.7
CGCG 108-053	17.8	3.9	4.6	14.3	-19.5	13.6	-20.2	1.0	6.8
NGC 6008B	14.2	4.3	5.1	14.6	-19.6	13.7	-20.4	1.2	...
NGC 6008	28.7	4.4	8.9	13.4	-20.6	12.8	-21.3	2.6	7.5
UGC 10197	24.4	0.9	1.5	14.4	-19.6	13.9	-20.1	0.9	0.09
UGC 10198	22.9	1.5	2.3	14.2	-19.8	13.8	-20.1	0.9	0.09
CGCG 137-037	10.9	2.6	2.9	14.8	-19.0	14.2	-19.6	0.6	3.0
NGC 6020	29.2	13.4	-20.4	12.6	-21.2	2.5	...
NGC 6060	45.2	6.5	10.7	12.3	-21.5	11.7	-22.2	5.9	5.3

Notes. Column 1: galaxy identification. Note that galaxies are ordered by distance away from SS as in Table 3. Column 2: diameter of $\mu_g = 25$ mag arcsec $^{-2}$ isophote in the g band. Column 3: diameter of $\mu_g = 21.5$ mag arcsec $^{-2}$ isophote in the g band. Column 4: diameter of $\mu_g = 21.8$ mag arcsec $^{-2}$ isophote in the g band. Column 5: total magnitude in the g band corrected for galactic and internal extinction and for redshift. Column 6: absolute magnitude in the g band. Column 7: total magnitude in the r band corrected for galactic and internal extinction and for redshift. Column 8: absolute magnitude in the r band. Column 9: total luminosity in the r band. Column 10: bulge luminosity in the r band.

Table 7
SS Apparent Magnitudes

HCG79	Our data		Our data		H1989a		R1991	RC3	N2000a
	g_{TC}^a	r_{TC}^a	B_{TC}^b	R_{TC}^b	R_I^c	B_{TC}^d	$m_R(\mu_R)^e$	B_{T0}^f	VR
a	14.6	13.9	15.0	13.7	13.5	14.3	13.5(22.0)	14.5	13.1
b	14.3	13.8	14.7	13.6	13.1	13.8	13.5(21.3)	14.2	12.9
c	15.2	14.8	15.5	14.7	14.2	14.7	14.4(21.9)	...	13.6
d	15.4	15.8	15.5	15.8	16.7	15.9	15.7(22.0)	...	15.8
f	16.6	16.1	16.8	16.5	15.4(21.6)	...	17.2

Notes.

^a Magnitude enclosed by the last concentric isophote in the g and r bands respectively corrected for galactic and internal extinction and for redshift.

^b Calculated using the transformation equations given in Lupton (2005), <http://www.sdss.org/dr4/algorithms/sdssUBVRITransform.html>: $B = g + 0.3130(g - r) + 0.2271$ and $R = r - 0.1837(g - r) - 0.0971$.

^c R magnitude within $\mu_R = 24$ R -mag arcsec $^{-2}$ isophote.

^d B_T asymptotic magnitude corrected for internal and external extinction.

^e m_R extending to R surface brightness μ_R .

^f Total “face-on” B magnitude, corrected for galactic and internal extinction and for redshift.

based measurements to H1989a, R1991, RC3, and N2000a. Our apparent magnitudes measure the light within the last concentric isophote corrected for galactic and internal extinction as well as K-corrected. Extinction corrections were performed using The York Extinction Solver (YES)¹⁷ (McCall 2004). YES allows the user to determine the optical depth at $1\mu\text{m}$ from an estimate of the color excess, and then to determine the extinction of the target from the optical depth. Color excess is estimated using Schlegel et al. (1998) extinction maps employing a Fitzpatrick (1999) reddening law.

Table 8 presents our g - and r -band absolute magnitudes and luminosities for SS galaxies. As noted earlier, the galaxies appear to be remarkably luminous for their small sizes which are more similar to the size of the bulges of late-type neighbors. Along with diameters, Table 6 presents absolute magnitudes, total luminosities, and bulge luminosities for the accordant

¹⁷ The York Extinction Solver (YES) at <http://cadwww.hia.nrc.ca/yes>.

Table 8
SS Absolute Magnitudes and Luminosities

HCG79	M_g	L_{gT} (10^9L_{\odot})	M_r	L_{rT} (10^9L_{\odot})
a	-19.3	4.2	-20.0	7.9
b	-19.6	5.5	-20.1	8.7
c	-18.7	2.4	-19.0	3.5
d	-18.5	2.0	-18.1	1.4
f	-17.3	0.7	-17.3	0.7

redshift neighboring galaxies. Overlapping structure in the close spiral pair NGC6052 prevents precise determination of their sizes and magnitudes. Other late-type neighbors (NGC6028 and CGCG108-085) lack any SDSS imaging data. Apparent magnitudes are corrected model magnitudes (modelMag- better of exponential/deVaucouleurs fit) given by the SDSS DR5 pipeline. The total luminosities in each filter were calculated

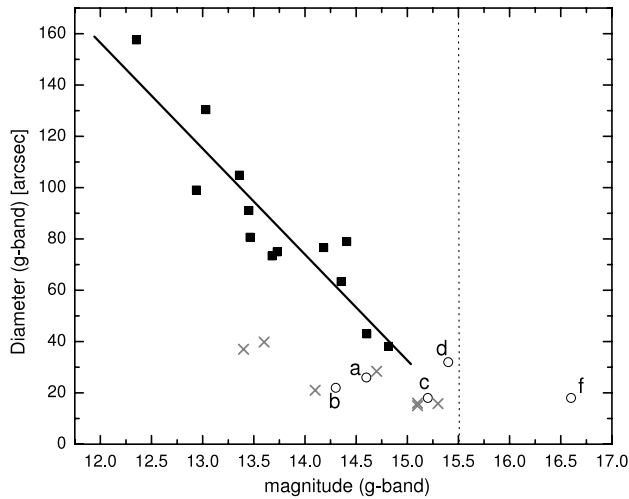


Figure 5. Size versus magnitude for neighbors (filled squares), bulges of SO and Sb-Sc neighbors (crosses), and galaxies in SS (open circles).

using the formulae

$$L_{gT} = 10^{0.4(M_{g\odot} - g_{rc} + 5 \log D - 5)} (L_{g\odot})$$

$$L_{rT} = 10^{0.4(M_{r\odot} - r_{rc} + 5 \log D - 5)} (L_{r\odot})$$

where $M_{g\odot} = 5.12$ and $M_{r\odot} = 4.68$ are adopted for g and r absolute magnitudes of the Sun, respectively. To express the luminosities in terms of bolometric solar luminosity we used $M_{\odot} = 4.76$ which implies ratios $L_{\odot}/L_{g\odot} = 1.39$ and $L_{\odot}/L_{r\odot} = 0.93$. The assumed distance is $D = 60$ Mpc. Bulge luminosities are estimated considering a bulge-to-disk ratio (B/D) ~ 1 for Sa, ~ 0.65 for Sab, ~ 0.4 for Sb, ~ 0.1 for Sc, and ~ 0.01 for Sd morphological type (Kent 1985; Köppen & Arimoto 1990) and the equation $B/T = 1/(1 + D/B)$, where T is the total luminosity. B/T is assumed to be 0.68 for SO morphological type (Kent 1985). Inspection of Tables 6 and 8 shows that the total luminosities of galaxies H79abc are comparable to the bulge luminosities of the Sb-Sc and SO neighbors.

Figure 5 plots apparent diameter versus g -band magnitude for SS galaxies (open circles) and 13 accordant redshift neighbors (filled squares): (1) within ± 1000 km s $^{-1}$, (2) within 2 Mpc radius and (3) brighter than $g = 15.5$. Measured diameters for the neighbors correspond to the 25 mag arcsec $^{-2}$ g -band isophote. We used the corrected modelMag values from the SDSS. We also plot the bulges for SO and Sb-Sc neighbors with sizes and magnitudes corresponding to the 21.8 mag arcsec $^{-2}$ g -band isophote. Diameters and magnitudes for SS components correspond to the last concentric g -band isophote. The plot shows the expected correlation between angular diameter and apparent magnitude for the accordant neighbors. It is reasonably well fitted by the indicated linear regression line. The brightest neighbor NGC6060 is similar in luminosity to M31 ($M_g \sim -21.5$), while H79d is similar to the LMC ($M_g \sim -18.2$). H79f, considered as a galaxy, would be 0.4 magnitudes fainter than the Small Magellanic Cloud (SMC) ($M_g \sim -16.9$). Apparent g -band magnitudes for M31, LMC, and SMC were estimated from V magnitude and $B - V$ color using the transformation equation $g = V + 0.6(B - V) - 0.12$ (Jester et al. 2005). Conversion to absolute magnitudes assumed distances of ~ 750 kpc for M31 (Ribas et al. 2005), ~ 50 kpc for LMC, and ~ 60 kpc for SMC (Keller & Wood 2006). SS members are smaller than all of the galaxies in our neighborhood sample.

Figure 5 shows that H79abc are similar in apparent brightness to the faintest neighbors, but they show much higher mean surface brightness. H79abc show g -band mean surface brightness within the last concentric isophote $\mu_g = 19.9$ – 21.1 mag arcsec $^{-2}$ compared to $\mu_g = 22.5$ – 23.5 mag arcsec $^{-2}$ calculated within the 25 mag arcsec $^{-2}$ isophote for their neighbors. The two neighbors with most similar size and apparent brightness show $\mu_g = 22.5$ – 22.9 mag arcsec $^{-2}$. Galaxies in SS show much higher mean surface brightness and are embedded in a luminous halo. Their size and surface brightness are more similar to the bulge components of neighboring spiral and SO neighbors. The mean surface brightness of one of the brightest neighboring Sb galaxies (NGC6008) would increase from 22.9 to 20.8 mag arcsec $^{-2}$, while the diameter would decrease from 1.5 to 0.2 arcmin if we considered only the central bulge. The overall mean surface brightness of SS is also high. It is by far the highest observed (20.5 mag arcsec $^{-2}$) for any H1982 group. Only three other groups (HCG8, 40, and 95) show values within one magnitude (21.3–21.4 mag arcsec $^{-2}$). Allowing for a different zero point in the surface brightness scale suggests that none of the 121 southern compact groups (Iovino 2002) approaches the surface brightness of SS.

Figure 6 is a composite of our B and R images showing the extension of the diffuse halo. According to D2005 the halo contributes $\sim 46\%$ of the total light in the B band (see also Sulentic & Lorre 1983). We get a similar result with g - and r -band SDSS images. The halo is a fraction of $46 \pm 10\%$ and $45 \pm 10\%$ of the total light in the g and r bands, respectively, if we do not include galaxy H79f as part of the halo. This corresponds to a corrected apparent magnitude of $g = 13.4 \pm 0.1$ and $r = 12.9 \pm 0.1$. If we included H79f, the halo contribution would raise by 2% in both g and r bands. We estimated the diffuse light in SQ using the magnitudes of the halo and component galaxies given in Moles et al. (1998). The diffuse light component represents $\sim 13\%$ of the total light, suggesting that SQ is a less evolved compact group, younger than SS. The early-type fraction in SQ is about 40–50%.

A diffuse light image was derived for SS using the wavelet technique (Figure 6 in D2005). The symmetry and smoothness of the halo light distribution in our Figure 6 suggests a reasonable degree of relaxation compared to, e.g., SQ. There are two peaks in the halo light distribution of SS. One is coincident with the NW tidal tail marked in Figure 6 of D2005. The other, which does not coincide with a galaxy or tail, lies much closer to the center of the diffuse light distribution. We attempted to model the radial profile of the CFHT B -band halo image (D2005) and find that an exponential yields the best fit. We get disk scale lengths $R_d = 23$ and 28 kpc, centered, respectively, on an approximate outer halo contour (circle in Figure 1 (left)) and on the SE condensation. We also attempted de Vaucouleurs and Sérsic fits on the surface-brightness profile of the halo. However, they could be applied only for the outer part and even so we obtained unphysical results, namely extreme values for the effective radii. While the overall halo is smooth and roughly circular, consistent with relaxation, the condensation connected with the tidal tail indicates that the halo is still growing.

3.1.4. Group Morphology and Colors

We supplement published color information on SS with our SDSS $g - r$ and our NOT $B - R$ measures. Table 9 lists new and old color measures for group members as well as the halo while Figure 7 shows our best attempt at a 2D $B - R$ color image. Tabular results are consistent with Figure 7. The central region

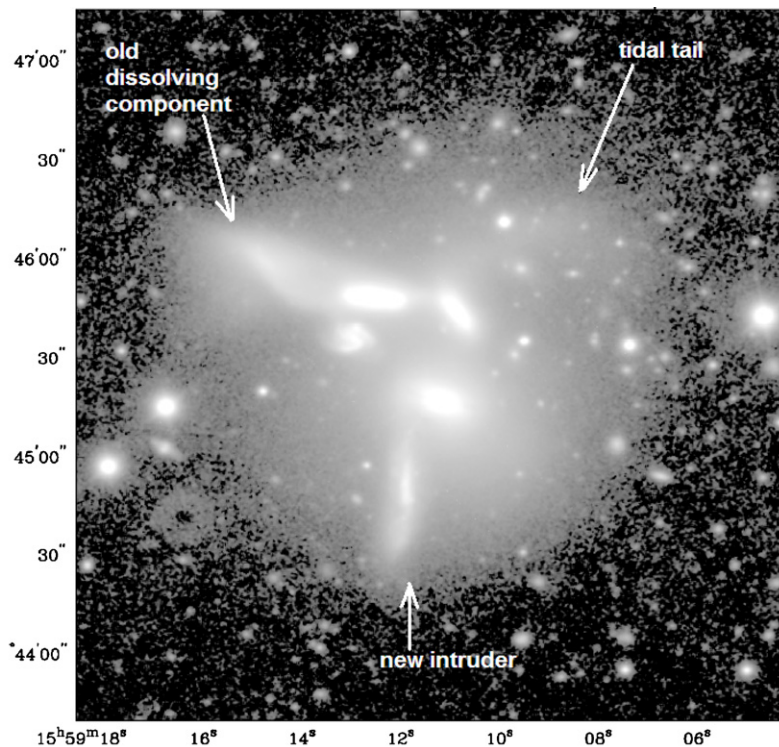


Figure 6. $B + R$ color image of SS.

Table 9
SS Colors

HCG79	Our data		H1989a
	$(g - r)_o$	$(B - R)_o$	$B - R$
a	0.6	1.3–1.8	1.6
b	0.5	1.3–1.5	1.4
c	0.4	1.2–1.3	1.3
d	–0.1	0.7–0.9	0.8
f	0.4	1.3–1.4	...
halo	0.4	0.8–1.3	...
NW tail	...	1.2–1.3	...

Notes. Column 1: galaxy identification. Column 2: $g - r$ color within the last concentric isophote (for galaxies abcd) in the r band (SDSS). The color does not change if we use the last concentric isophote in the g band. Column 3: $B - R$ color (NOT). Column 4: $B - R$ color within the $\mu_B = 24.5$ mag arcsec^{-2} isophote (Hickson et al. 1989a).

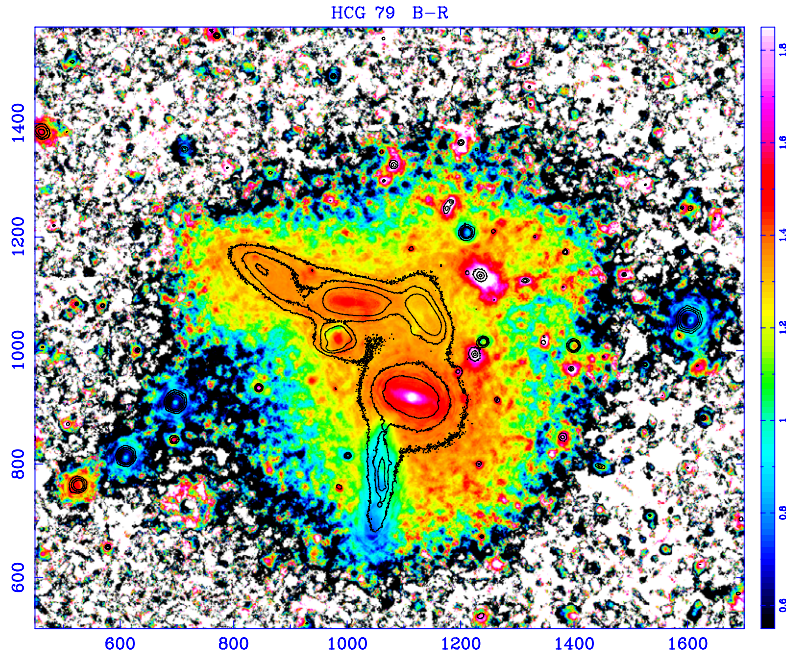
of H79a shows the reddest color ($B - R \sim 1.6$ – 1.8) due to the presence of the strong dust lane. The inner parts of galaxies H79a/b show $B - R \sim 1.5$ which is typical of an early-type or bulge stellar population. The outer parts of galaxies H79a/b as well as H79f show $B - R \sim 1.3$ – 1.4 . The color of galaxy H79f is in good agreement with Nishiura et al. (2002). Galaxy H79c, much of the diffuse halo as the NW tidal tail show $B - R \sim 1.2$ – 1.3 while the outer halo is distinctly bluer at $B - R \sim 0.8$ – 1.1 . All results indicate that galaxy H79c is bluer than galaxies H79a/b with complex color structure. It is bluest on the side towards the center of the group. The bluest colors are seen in galaxy H79d with $B - R \sim 0.7$ – 0.9 which is typical of a late-type spiral. We see a slight color difference $\Delta(B - R) = 0.3$ along the

major axis with reddest color in the direction of galaxy H79a.

Color measures for the halo component are the most complex. We find a mean halo color that is bluer than galaxies H79a/b and more similar to galaxies H79c/f. D2005 also reported a much bluer color for the halo $B - R = 0.9$ compared to $B - R = 1.5$ for the galaxies. We derived halo properties after subtracting galaxies at their last concentric isophote which might leave a significant red galaxy component in our halo measures. The wavelet technique employed for the D2005 estimates more effectively removes the galaxies leaving a much flatter halo. The resultant galaxy color will be dominated by red galaxies H79a/b. The wavelet derived halo color is similar to galaxy H79d. Figure 7 suggests that the halo shows a significant color gradient and that the outer parts are as blue as those of a late-type spiral. If the mean color of H79d is $B - R = 0.8$, then we can adopt a mean halo color of $B - R = 1.0 \pm 0.2$ as a best estimate. $B - R$ colors were only corrected for galactic extinction using Burstein & Heiles (1982). Other corrections are very dependent on the morphological type, which is uncertain for some members of the group. An internal extinction correction for galaxy H79d (morphological type Sd) would make it $0.2 B - R$ magnitudes brighter. The color of the outermost halo isophotes will be sensitive to the S/N match between the B and R frames; our estimate based on the intermediate halo color is likely to be more robust.

3.2. Optical Line ($H\alpha$ Emission)

Figure 8 presents a continuum subtracted $H\alpha$ image derived from the CFHT Fabry–Pérot observations. Figure 9 shows a similar continuum-subtracted interference filter (IF) image obtained with the Calar Alto 2.2 m telescope that confirms all features seen in Figure 8. The former provides higher sensitivity and resolution, while the latter image gives a much larger FOV that allows a search to be made for stripped warm gas or gas-rich

Figure 7. $B - R$ color image of SS.Table 10
SS $H\alpha$ Fluxes

HCG79	Our data ¹	Our data ²	I&V1999 ^{a,1}	Our data ²	C2004 ^{b,2}	N2000a ^{c,2}	S2000 ^{d,3}
	$\log f_{H\alpha+[N II]}$ ($\text{erg s}^{-1} \text{cm}^{-2}$)			$\log f_{H\alpha}$ ($\text{erg s}^{-1} \text{cm}^{-2}$)			
a	-13.65	...	-13.58	...	-13.99	-14.60	(-15.04)
b	-13.56	-13.54	-13.56	-13.71	-13.62	-14.00	(-14.20)
c	<-16.53	abs	<-16.91	abs	...	abs	abs
d	-13.64	-13.93	-14.05	-13.90	-15.33	-14.75	(-15.25)

Notes. ¹ From reduced $H\alpha$ interference filter image. ² From long-slit spectra. ³ From nuclear spectra. abs denotes absorption.

References. ^a Iglesias-Páramo & Vílchez (1999); ^b Coziol et al. (2004); ^c Nishiura et al. (2000a); ^d Shimada et al. (2000).

companions. In this section we use the 3D CFHT data only as the source of an additional 2D $H\alpha$ map. $H\alpha$ emission is detected from galaxies H79a, b, and d. Emission is detected over the full optical extent of galaxy H79d, while emission from H79a and b is detected only in the central regions. The weak emission signature associated with H79c is not confirmed with our slit spectra and is likely an artifact of the strong Balmer absorption detected in that galaxy.

Table 10 summarizes new and published $H\alpha$ fluxes for these galaxies including both IF and slit spectral measures. The former include a contribution from $[N II] \lambda 6548,83$ emission. Our flux measures have an uncertainty lower than $\pm 10\%$, computed as Poissonian error. We find a large scatter among published EW $H\alpha$ ($+ [N II] \lambda 6548,83$) measures: 1–7 Å, 4–8 Å, and 13–116 Å (N2000a; Iglesias-Páramo & Vílchez 1999; Coziol et al. 2004) for galaxies H79a, b, and d, respectively. We measure 10 Å, 9 Å, and 36 Å, respectively, for the three galaxies. $[N II]$ contamination could not be avoided with the IF filter employed (FWHM = 76 Å). Typical EW for E/SO galaxies range from –3 to 4 Å (Kennicutt Jr. 1998). Our EW measure for H79d is similar to published values for normal Sd galaxies (Kennicutt Jr.

1998; James et al. 2004). A mean EW $H\alpha$ = 36 Å was found in a recent study involving Sd galaxies (James et al. 2004). $H\alpha$ flux measures for H79d tabulated in Table 10 show much less scatter than EW estimates reflecting the uncertainty of the continuum normalization for this late-type edge-on galaxy. We estimate a star formation rate (SFR = $0.07 M_{\odot} \text{ yr}^{-1}$) which is smaller than the mean value ($0.6 M_{\odot} \text{ yr}^{-1}$) found for normal Sd spirals (Kennicutt Jr. 1983; James et al. 2004). SFR is computed using the formula derived for normal disk galaxies:

$$\text{SFR}(M_{\odot} \text{ yr}^{-1}) = 7.9 \times 10^{-42} L(H\alpha) (\text{ergs}^{-1})$$

assuming a Salpeter (1955) initial mass function (IMF) with mass limits 0.1 and $100 M_{\odot}$ (Kennicutt Jr. 1998). We derived the net $H\alpha$ luminosities using the $[N II] \lambda 6583/H\alpha$ line ratios from N2000a. The SFR for H79d increases to ~ 0.11 if we apply the same (1.1 magnitude) extinction correction as used in James et al. (2004). $H\alpha$ flux and derived SFR values for H79d therefore show no evidence for an interaction induced enhancement.

Using the same formula we estimate SFR ~ 0.05 and $0.06 M_{\odot} \text{ yr}^{-1}$ for galaxies H79a and b, respectively. The

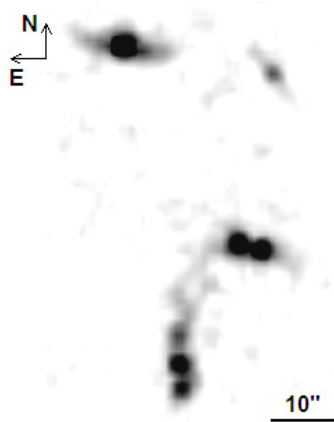


Figure 8. MOS/SIS Fabry-Pérot (CFHT 3.6 m) continuum-subtracted $H\alpha$ image: sum of five velocity channels, corresponding to velocities in the range 4350–4395 km s⁻¹ (galaxy H79a) in 0 interference order and 4615–4660 km s⁻¹ (galaxy H79d) in +1 interference order.

[N II]λ6583/ $H\alpha$ line ratio is ~ 0.5 for both galaxies (N2000a) which is at the lower limit of the typical values (0.5–3) found for early-type galaxies (Phillips et al. 1986). $H\alpha$ emission in galaxies H79a and b shows an extension on a scale of 3–4 kpc, larger than the typical size of $H\alpha$ emission regions in early-type galaxies (<3 kpc) (Phillips et al. 1986). Apparently there is too much gas in H79a/b if they are interpreted as normal SO galaxies. The emission in H79a shows two condensations separated by 3'' superimposed on weaker more extended emission. One component (NE) is coincident with or slightly E of the position of the optical nucleus and lies at the end of an apparent emission “bridge” between H79d and H79a that can be seen in Figure 8. The other component (SW) is about 0.74 times the intensity of the NE component. Galaxy H79b shows a compact central emission component with diameter $D \sim 5''$ superimposed on a weak elongated diffuse component with major axis diameter $D \sim 15''$. The latter component shows distinct curvature or warping. The central component appears to be slightly offset towards the N on Figure 8.

We estimated the mass of ionized gas following Phillips et al. (1986), where

$$M_{\text{ionized gas}} = (L_{H\alpha} m_H / N_e) / (4\pi j_{H\alpha} / N_e N_p),$$

where $L_{H\alpha}$ is the $H\alpha$ luminosity, m_H is the mass of the hydrogen atom, $j_{H\alpha}$ is the $H\alpha$ emissivity, N_e and N_p are the electron and proton densities, respectively. The assumed electron temperature was 10⁴ K. The [S II] λ6717/λ6731 line ratio was used as an electron density indicator (Osterbrock & Ferland 2006). [S II] λ6717/λ6731 line ratios for galaxies H79b and d are estimated from our slit spectra and are tabulated in Table 11 along with other line ratios. No [S II] λ6717/λ6731 line ratio exists for galaxy H79a so we adopted the same ratio as galaxy H79b. The value for $4\pi j_{H\alpha} / N_e N_p$ was derived using the H I recombination line tables of Osterbrock & Ferland (2006). The computed ionized gas masses are $7.5 \times 10^4 M_\odot$, $9.2 \times 10^4 M_\odot$, $3.5 \times 10^5 M_\odot$ for galaxies H79a, b, and d, respectively. The ionized gas masses for galaxies H79a and b are within the range of values (between 10³ and 10⁵ M_\odot) found by Macchetto et al. (1996) for luminous elliptical and lenticular galaxies. On the other hand Phillips et al. (1986), using a larger sample of early-type galaxies, report a mean value between 10³ and 10⁴ M_\odot . This would place galaxies H79a and b at the upper

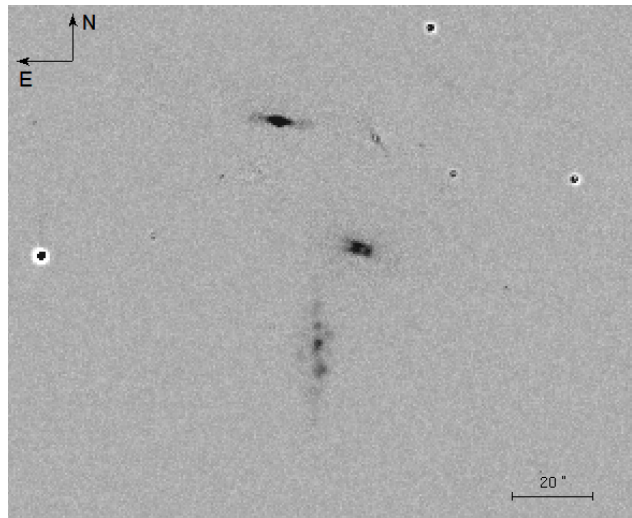


Figure 9. Continuum-subtracted $H\alpha$ interference filter image centered at 6667 Å of SS.

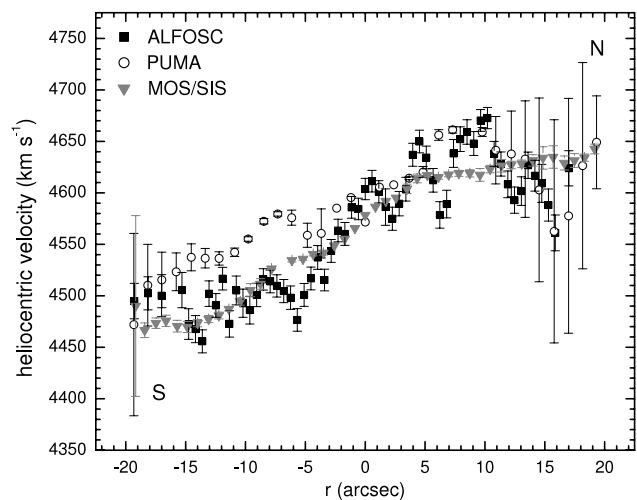


Figure 10. H79d line of sight velocity curve along major axis (PA = 180°—PUMA & MOS/SIS; PA = 179.3°—ALFOSC).

end of the distribution of ionized gas masses for early-type galaxies. Emission line diagnostic diagrams of Kewley et al. (2006) suggest that much of the gas in H79a may be related to the AGN rather than to star formation so the already uncertain estimated mass may be too high. The [O III]/ $H\beta$ line ratio of Coziol et al. (2004) is used.

We used the larger field of view of our PUMA (10' × 10') and Calar Alto (13' × 5') observations to search for $H\alpha$ emission from other galaxies in the field that might represent previously unknown neighbors of SS. The search was performed two different ways: using ADHOCw software and the IRAF task DAOFIND imposing a threshold of 4σ. No candidates were found implying that no gas-rich dwarf systems similar to H79d lie within ~ 90 kpc. We also looked for discrete $H\alpha$ condensations similar to the ones found in the debris field of SQ (Sulentic et al. 2001). We required confirmation on at least two independent $H\alpha$ images with agreement within a few arcseconds to allow for field distortion.

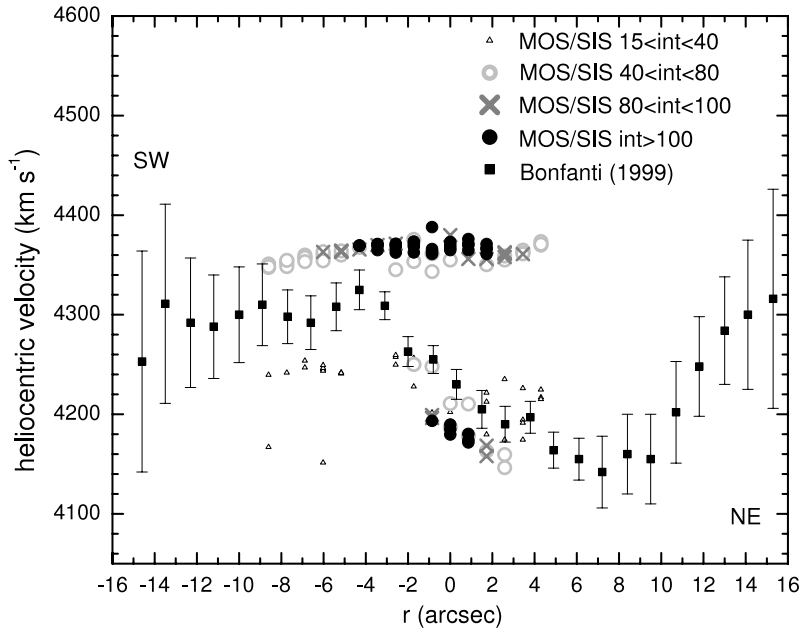


Figure 11. H79a line-of-sight velocity curve along major axis (PA = 65°) the “int” corresponds to the intensity of the peak of each component.

Table 11
SS Spectroscopic Measures

HCG79	$\frac{[N\text{ III}]\lambda 6584}{H\alpha}$	$\frac{[S\text{ II}]\lambda 6717.31}{H\alpha}$	$\frac{[S\text{ II}]\lambda 6717}{[S\text{ II}]\lambda 6731}$	$EW(H\alpha)$	$EW([N\text{ III}])$
a
b	0.47±0.01	0.33±0.01	1.25±0.01	12.74±0.64	5.80±0.25
c	abs	abs	abs	abs	abs
d	0.15±0.02	0.38±0.02	1.37±0.06	48.50±3.00	3.50±0.30

Note. abs denotes absorption; all the values in the table are obtained from our long-slit spectra.

3.3. Optical Spectroscopy

3.3.1. H α Emission

H79d is the only galaxy in SS that shows a normal late-type ISM. Figure 10 compares new Fabry–Pérot (FP) and slit H α line-of-sight velocity curves. They show good agreement (also with R1991; Mendes de Oliveira et al. 2003; Nishiura et al. 2000b) when differing spatial/spectral resolutions are taken into account. The rotation curves are not strongly distorted suggesting (along with gas content) that H79d is a relatively recent arrival without evidence of strong perturbation. Figure 10 suggests a reasonable estimate for the maximum rotation velocity v_{\max} for galaxy H79d is $\sim 100\text{ km s}^{-1}$ after correction for 80° inclination. Using v_{\max} we derive a mass within 13'' radius ($R \sim 3.8\text{ kpc}$) of $\sim 9 \times 10^9 M_{\odot}$, thus $(M/L_r)_{H79d} \sim 6 M_{\odot}/L_{\odot}$. R1991 find the mass to R_{25} for H79d $\sim 3 \times 10^{10} M_{\odot}$ and $(M/L_B)_{H79d} \sim 3.7 M_{\odot}/L_{\odot}$, using the mass and luminosity within R_{25} , radius corresponding to 25 mag arcsec $^{-2}$ in the B band.

Figure 11 presents the line-of-sight velocity curve for H79a. We plot the heliocentric velocity along the major axis of the H α emission from FP interferometry using CFHT-MOS/SIS data. Our PUMA measures were indispensable in interpreting the higher resolution and S/N CFHT ones. PUMA has more than three times the free spectral range of CFHT and was able to resolve the order overlap that affected the higher resolution and S/N CFHT measures. The larger free spectral range of our

PUMA data was used to resolve velocity redundancy inherent in the higher-sensitivity CFHT FP data. A published stellar velocity curve based on long-slit observations (Bonfanti et al. 1999) is superimposed on this plot. In order to match the long-slit data, we mimic a slit through our FP data at PA = 65°. We find two H α velocity components: (1) a weak and compact ($\sim 5''$) nuclear component with velocities ($\sim 4180\text{ km s}^{-1}$) very similar to stellar values in the nuclear region (this is part of the NE spatial component in Figure 8) and (2) a more extended (at least $\sim 8''$) higher-velocity ($\sim 4360\text{ km s}^{-1}$) component (part of NE and all of SW components in Figure 8). The NE spatial component is more intense because it involves H α emission from both velocity components. The infalling emission shows almost constant velocity that, at the center, is $\sim 150\text{ km s}^{-1}$ higher than the starlight. The match with the stellar velocity curve suggests that velocity component (1) is nuclear gas and that velocity component (2) can be interpreted as an infalling sheet of gas.

The infalling gas in H79a is either evidence for feedback from earlier stripping episodes in SS or cross-fuelling from a gas-rich neighbor. H79d is the obvious candidate if one considers the latter interpretation, and it is supported by the apparent H α bridge between H79a and d that is shown in Figure 8, which shows the sum of five velocity channels from the MOS/SIS continuum subtracted image. This corresponds to velocity range 4350–4395 km s^{-1} in the zeroth order and 4615–4660 km s^{-1} in the first order. These velocities are consistent with emission

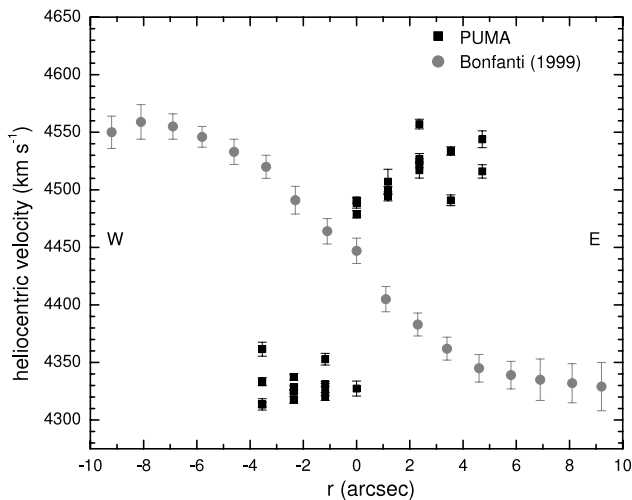


Figure 12. H79b line-of-sight velocity curve along the direction connecting the nuclei of galaxies H79bc ($PA = 79^\circ$).

from both H79a and H79d. While we see an apparent bridge (see also R1991) between galaxies H79a/d we do not find velocity continuity. The northernmost condensations in H79d can be seen in silhouette on the outskirts of H79a (Palma et al. 2002). The rotation curve of H79d shows velocities $\sim 4650 \text{ km s}^{-1}$ near this overlap zone. This is about 500 km s^{-1} higher than the nuclear gas in H79a and $\sim 300 \text{ km s}^{-1}$ higher than the infalling $H\alpha$ component in that galaxy. If the infalling gas in H79a originated in H79d then the fuelling was episodic and not continuous. If H79d did not provide the fuel then feedback of gas previously stripped from SS members would likely be the source. Using a velocity dispersion $\sigma_0 \sim 155 \text{ km s}^{-1}$ (Bonfanti et al. 1999) we get a mass for H79a within $14''$ (last concentric isophote) $\sim 10^{10} - 10^{11} M_\odot$.

Figure 12 presents the line of sight velocity curve for H79b with our new SPM-PUMA data. In this case we find a well-defined $H\alpha$ emission rotation curve that is counter-rotating relative to the stellar velocity curve from Bonfanti et al. (1999). This is evidence for a minor or quiet (lacking a strong MIR/FIR (far-infrared) signature) merger as suggested by Sulentic et al. (1994). Figure 13 shows the counter-rotation of the $H\alpha$ gas in galaxy H79b relative to Bonfanti et al. (1999) and our new stellar velocity curve obtained with ALFOSC. The estimated mass of H79b within $11''$ (\sim the last concentric isophote) is in the range $9.0 \times 10^9 - 1.7 \times 10^{10} M_\odot$ using the Bonfanti et al. (1999) and ALFOSC rotation curves (Figure 13), respectively. This is an underestimation of both the current mass and, much more, the original mass of H79b. Our estimates of the mass-to-light ratio range from 1 to 2. If H79b entered SS as an L^* galaxy then it has lost 50–90% of its original mass into the common halo. It has gained the mass of the counter-rotating component estimated from the $H\alpha$ velocity curve to be $\sim 3.3 \times 10^9 M_\odot$. The latter value suggests that H79b accreted a late-type dwarf intruder somewhat less massive than H79d. The lack of $H\alpha$ field detections suggest that no new intruders will visit SS in a significant fraction of the next Gyr.

We attempted to obtain velocity dispersion measures for several of the galaxies, but our spectral resolution was too low to yield useful measures except in the case of H79c. Previous measures of $\sigma = 155, 130,$ and 60 km s^{-1} for H79a, b, and c, respectively (Bonfanti et al. 1999) all fall close to the

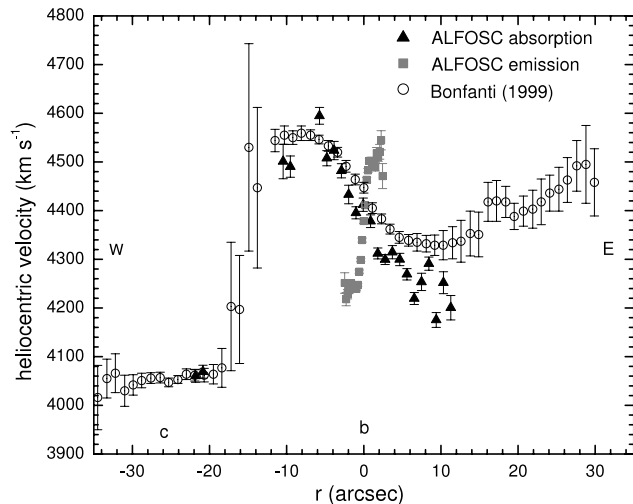


Figure 13. Line-of-sight velocity curve along the direction connecting the nuclei of galaxies H79bc ($PA = 79^\circ$ —Bonfanti et al. (1999); $PA = 81^\circ$ —ALFOSC).

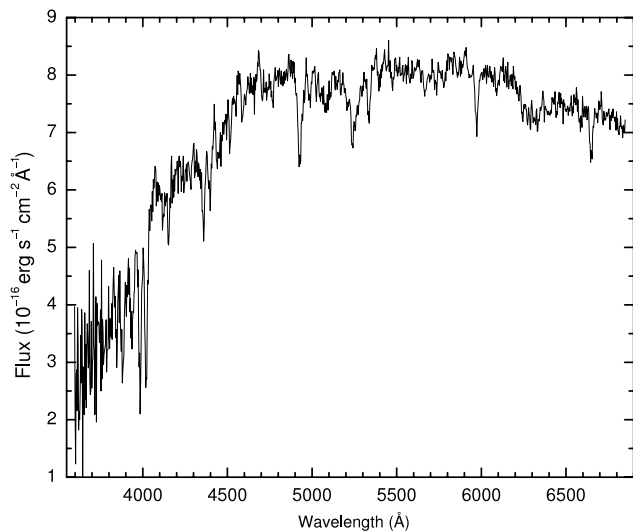


Figure 14. Spectrum along the slit of galaxy H79c corresponding to an aperture of $12''$ ($PA = 35^\circ$).

fundamental plane of elliptical galaxies (see Figure 7 in de la Rosa et al. 2001) and close to a $\sigma - M_B$ relation defined for dwarf/giant elliptical galaxies, galactic bulges, and dwarf spheroidals (Bender et al. 1992). H79c, which shows properties least like an elliptical galaxy, also shows the largest deviation from the $\sigma - M_B$ relation in the sense that the velocity dispersion is too low. Our corrected estimate for H79c is slightly higher at $\sigma = 89 \text{ km s}^{-1}$.

3.3.2. $H\alpha$ Absorption

Figure 14 shows the slit spectrum of galaxy H79c. We attempted several different estimates for the age of galaxy H79c. (1) We fitted the spectrum with theoretical templates (Bruzual & Charlot 2003) computed for different stellar populations and metallicities. The best-fit template corresponds to a stellar population of $\sim 1.5 \text{ Gyr}$ with metallicities of both $Z = Z_\odot = 0.02$ and $Z = 0.05$. (2) Using the program indexf (Cardiel et al. see <http://www.ucm.es/info/Astrof/users/ncl/index.html>) we derived some age indices (e.g. $D_n(4000)$, $H\delta_A$, $Fe5015$, etc.)

that are commonly used to date galaxy stellar populations (e.g. Kauffmann et al. 2003; González Delgado et al. 2005; de la Rosa et al. 2007). We obtained $D_n(4000) = 1.56$, $H\delta_A = 2.09$, $Fe5015 = 3.44$, $H\beta = 3.18$, $D(4000) = 1.83$, $Fe5406 = 0.88$. We performed also simulations (photon counting) on the spectrum to get an estimate of the errors in the indices due to S/N: for example, for $D_n(4000)$ such errors are ~ 0.01 – 0.02 and for $H\delta_A$ are ~ 0.5 – 0.08 . Following Kauffmann et al. (2003) (see their Figure 2), we estimate that H79c had its last burst of star formation ~ 1.5 – 1.8 Gyr ago (if an instantaneous, solar-metallicity burst model is considered). The estimates are still consistent if bursts of different metallicities are considered. (3) The value of $D(4000) = 1.83$ seems to be unreliable in getting age estimates. While $D_n(4000)$ and $H\delta_A$ indices are in agreement according to Figure 3 of Kauffmann et al. (2003), $D(4000)$ and $H\delta_A$ do not match any of the models illustrated in Figure 9 of González Delgado et al. (2005). (4) Figure 3 of Proctor et al. (2004) shows index–velocity–dispersion relations. With its estimated $\sigma = 89$ km s $^{-1}$ the location of H79c in such plots would infer a spiral bulge behavior, rather than an S0. Using their Figure 4 the age estimate is ~ 2 – 3 Gyr and $[Fe/H] \sim -0.75$. All these methods used to estimate the age lead to an average age of ~ 2 Gyr for H79c. This relatively young age is consistent with the bluer colors reported earlier for galaxy H79c and with the hypothesis that H79c is a stripped spiral that intruded into the group near that time. It was likely the intruder that preceded H79d. At the other extreme a lower S/N spectrum of H79f is consistent with a much older age consistent with its being one of the original group members now in a stage of dissolution.

3.4. MIR/FIR

Compact groups generally show depressed levels of FIR emission because the component galaxies quickly lose their ISM to encounters and collisions (Sulentic & de Mello Rabaça 1993). Only recently formed groups or transient systems would be expected to show normal or above normal emission. SQ revealed low levels of star formation igniting in the tidal debris (Sulentic et al. 2001) with very little emission in the component galaxies. The expectation for SS, viewed as significantly more evolved than SQ, would be that only recent unstripped intruders might show significant FIR emission with a possible component from the debris field. Our H α search failed to find evidence for the latter component. The situation is different for MIR emission where quasi-continuous interactions might efficiently channel any residual unstripped gas into component nuclei. Thus MIR emission from a warm ISM (H II regions) would not be expected while nuclear sources, sometimes connected with AGN, could be common. SQ tells us that warmer emission from large-scale shocks or debris field starbursts can also occur. We must rely upon the *IRAS* survey for information about FIR emission in SS while a new ISO map provides insights into the MIR emission.

SS shows moderate FIR emission (Verdes-Montenegro et al. 1998) with estimated $L_{FIR} \sim 8.7 \times 10^9 L_{\odot}$ reflecting *IRAS* fluxes at 60 and 100 μm $S_{60} = 1.28$ Jy and $S_{100} = 2.82$ Jy, respectively. FIR luminosity is computed using $\log(L_{FIR}/L_{\odot}) = \log \text{FIR} + 2 \log D + 19.495$, where $\text{FIR} = 1.26 \times 10^{-14} (2.58 S_{60} \mu\text{m} + S_{100} \mu\text{m}) \text{ W m}^{-2}$ (Helou et al. 1988), D is the distance in Mpc and $S_{60} \mu\text{m}$ and $S_{100} \mu\text{m}$ are the fluxes at 60 μm and 100 μm , respectively expressed in Jy. FIR luminosity is similar to the mean value for the most isolated luminous Sc spirals in the local Universe (Lisenfeld et al. 2007). SS is smaller than the *IRAS* beams at the 25 (3 – 4σ), 60, and 100 μm wavelengths

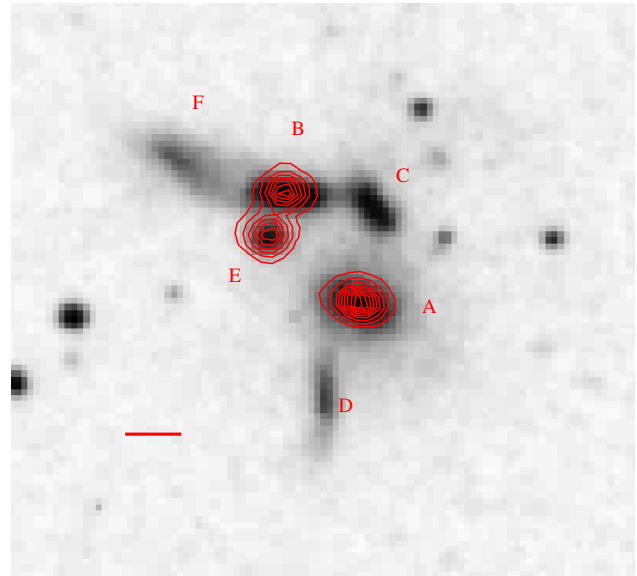


Figure 15. Isophotal contours of the LW10 ISOCAM image of SS superimposed on a DPOSS image of the same group. The contours drawn go from 4 to 5.5 mJy per pixel, in steps of 0.15 mJy. The background level is around 3.8 mJy per pixel. The horizontal bar on the left shows the aperture radius adopted to measure the fluxes reported in Table 12.

(A color version of this figure is available in the online journal)

Table 12
SS MIR Fluxes

HCG79	$S_{11.5 \mu\text{m}}$ (mJy)
a	18.2
b	12.7
e	12.5

where SS is detected. *IRAS* processing yields only unresolved detections although various studies have assigned the FIR emission to one or more members (Hickson et al. 1989b; Allam et al. 1996; Verdes-Montenegro et al. 1998). While the *IRAS* resolution was $\theta \geq 1'$ the pointing accuracy was much higher for strong detections. The 1σ position uncertainty ellipse for the SS detection was $12'' \times 4''$ (PA $\sim 100^\circ$) centered E of H79a and S of H79e. This is inconsistent with our expectation that H79d should dominate the FIR emission. It is almost certainly a significant contributor however several other sources of cold dust emission could be present, e.g., (1) H79a: the dust lane and/or the near-nuclear H α blobs, (2) H79b: the counter-rotating component and twisted dust lane, (3) H79e: as a luminous background ScI spiral and (4) possible diffuse dust emission associated with stripped H I near the *IRAS* position.

We described earlier new ISO MIR observations of SS, which are shown in Figure 15 as an 11.5 μm ISOCAM map with $6''$ resolution superimposed on a DPOSS optical image. We resolve SS into three sources involving H79a, b, and e. Photometry was performed with the IRAF APPHOT package where we interactively derived fluxes for the three sources present in the field adopting aperture photometry for our measures. For galaxies H79b and e, which are very close to each other, we masked galaxy H79b/e when measuring aperture photometry for galaxy H79e/b. Fluxes are listed in Table 12 and correspond to a total flux from the group that is roughly a factor of 2 below the *IRAS* upper limit of 90 mJy quoted in Moshir et al. (1990), while each galaxy flux is again a factor of 2/3 below the flux

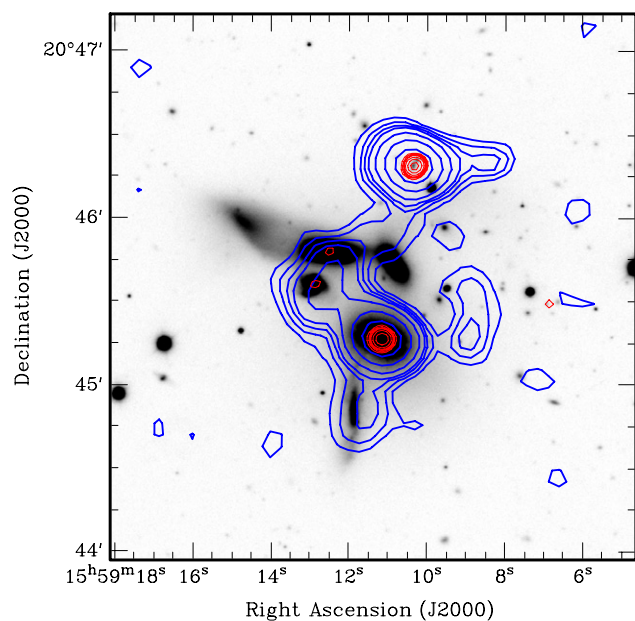


Figure 16. VLA: (bold contours) C-array 1.4 GHz radio continuum; (thin contours:) B-array 1.4 GHz radio continuum.

(A color version of this figure is available in the online journal)

limit estimated from the $12\ \mu\text{m}$ MaxEnt *IRAS* map of Allam et al. (1996). The lack of an $11.5\ \mu\text{m}$ detection for H79d is not surprising because late-type spirals tend to show a colder ISM. At the same time a massive and 4.5 times more distant ScI spiral-like H79e was detected by ISOCAM. MIR emission might be attributed to the active nucleus in H79a and to the accretion event in H79b.

The blue and FIR luminosities of the neighbors detected by *IRAS* are presented in Table 13. All of them fall on the L_B versus L_{FIR} correlation defined for isolated galaxies (Perea et al. 1997; Lisenfeld et al. 2007), except the pair UGC10197-8 which shows enhanced FIR emission as expected. If we assume that all of the FIR emission ($\log(L_{\text{FIR}}/L_{\odot}) = 9.93$) belongs to H79d that would imply that it is about 27 times brighter than the isolated galaxy expectation (~ 8.5) for sources of similar morphology and optical luminosity. There are two possible scenarios: either the emission in galaxy H79d is enhanced by interaction with the rest of SS or the FIR emission arises from several of the sources listed above.

3.5. Radio Continuum

A combined analysis of VLA (old and new data), NVSS¹⁸ and FIRST¹⁹ provides a clear picture about the sources of radio continuum emission in SS. VLA (see Figure 16) and NVSS isophotes indicate that the center of the emission lies closest to H79a. The archival VLA B-array image ($6''$ resolution) shows that three galaxies (H79a, b, and e) are reasonably compact radio sources with only H79a detected by FIRST. H79d is only detected with the C-array observations while H79b and e are blended together (see Figure 16). The photometry shows that the B-array data is missing some extended flux (see Table 14).

¹⁸ NRAO VLA Sky Survey (NVSS) is found on the web at <http://www.cv.nrao.edu/nvss/> (see also Condon et al. (1998))

¹⁹ Faint Images of the Radio Sky at Twenty-centimeters (FIRST) is found on the web at <http://sundog.stsci.edu/>.

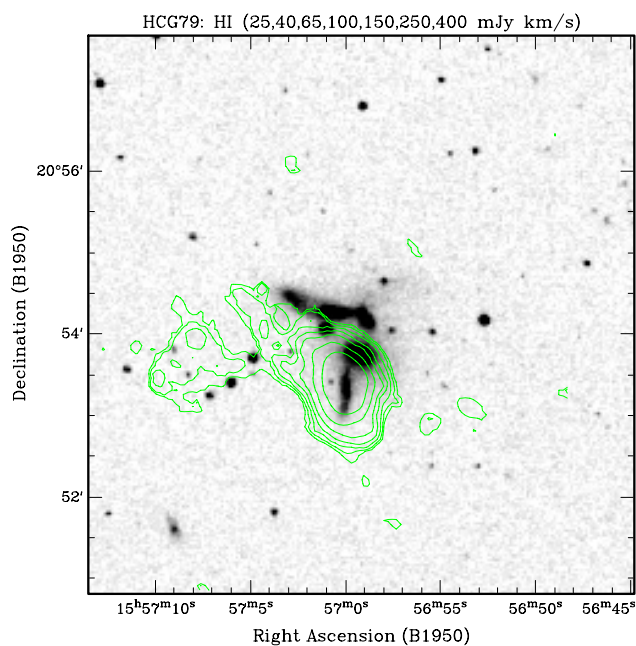


Figure 17. VLA: HI contours.

(A color version of this figure is available in the online journal)

This is not surprising if the emission from H79b, d, and e is connected with star formation in those galaxies

We also detect an apparently unrelated source $\sim 1'$ north of the group and near the tidal tail. It shows an integrated C-array flux of 5.9 mJy in agreement with FIRST, NVSS, Williams et al. (1991) and Dickel et al. (1984) measures. The optical counterpart appears to be one component of a distant interacting galaxy pair that is clearly resolved on *HST* images. The ~ 1 mJy source west of the group shows no optical counterpart.

We explore the well-known radio-FIR correlation (Dickey & Salpeter 1984) in order to estimate/resolve the FIR flux from galaxies in SS. A complete sample of 250 normal spiral galaxies brighter than $B = 12$ (Condon et al. 1991) shows the following strong correlation:

$$\log(L_{1.4\ \text{GHz}}[\text{WHz}^{-1}]) = 1.29 \log(L_{\text{FIR}}[L_{\odot}]) + 8.76$$

(we adapted the coefficients for $H_0 = 75\ \text{km s}^{-1}\ \text{Mpc}^{-1}$). If we assume that radio emission from H79b, d, e is dominated by star-formation-related processes then we expect that H79b and d each account for 25% of the total FIR flux with galaxy H79e accounting for 15%. The residual FIR emission is attributed to H79a (25–35%) involving, perhaps, emission from the AGN, star formation and the strong dust lane. Using the predicted FIR fluxes we find that all galaxies fall close to the FIR–optical correlation found by Lisenfeld et al. (2007) for very isolated galaxies.

We also explore the radio continuum–MIR correlation using ISO MIR and C-array radio continuum fluxes from Tables 11 and 13, respectively. Galaxies H79b and H79e closely follow the correlation found in Gruppioni et al. (2003). Galaxy H79a falls somewhat above the correlation showing excess radio continuum flux likely associated with the AGN.

3.6. Radio Line (21cm)

Williams et al. (1991) presented HI velocity channel maps for SS. The emission was centered on H79d with weak emission

Table 13
Neighbors Blue and FIR Luminosities

Galaxy	B_{T0}	$\log L_B$ (L_\odot)	$S_{60 \mu\text{m}}$ (Jy)	$S_{100 \mu\text{m}}$ (Jy)	$\log L_{\text{FIR}}$ (L_\odot)
UGC 10127	13.5 ^a	10.06	1.25	3.57	9.98
UGC 10117	14.5 ^a	9.66	0.29	0.91	9.37
NGC 6032	13.7 ^a	9.98	0.42	0.98	9.47
NGC 6008	13.6 ^a	10.02	0.51	2.07	9.68
UGC 10197	14.8 ^b	9.54	0.24	1.09	9.38
UGC 10198	14.5 ^b	9.65	0.24	1.09	9.38
NGC 6020	13.7 ^a	9.98	<0.03	<0.19	<8.59
NGC 6060	13.1 ^a	10.21	1.52	4.91	10.10
CGCG 108-085	15.4 ^a	9.30	0.61	1.44	9.63

Notes. Column 1: galaxy identification. Column 2: B_T asymptotic magnitude corrected for Galactic and internal extinction and K -corrected. Column 3: logarithm of the blue luminosity. Column 4: *IRAS* flux density at 60 μm . Column 5: *IRAS* flux density at 100 μm . Column 6: logarithm of FIR luminosity, obtained as explained in Section 3.4. Upper limits are indicated with < in front of the value.

^a Total blue magnitudes from RC3.

^b Calculated from g and r modelMag from the SDSS using the transformation equations given in Lupton (2005)- <http://www.sdss.org/dr4/algorithms/sdssUBVRITransform.html>: $B = g + 0.3130(g - r) + 0.2271$.

Table 14
Summary of 1.4 GHz Radio Continuum Sources in SS

	B -array	C -array	Notes
HCG79a	4.9 ± 0.7 mJy	6.9 ± 1.0 mJy	
HCG79b+e	1.1 ± 0.1 mJy	3.4 ± 0.5 mJy	
HCG79b	0.41 ± 0.07 mJy		
HCG79e	0.69 ± 0.10 mJy		
HCG79c	<0.2 mJy	<0.6 mJy	3σ limits
HCG79d	<0.2 mJy	1.4 ± 0.2 mJy	
Source W	<0.2 mJy	1.0 ± 0.2 mJy	No optical counterpart
Source N	5.7 ± 0.9 mJy	5.9 ± 0.9 mJy	A compact optical counterpart

Note. Uncertainties quoted are either a 1σ noise estimate in the continuum map or the 15% absolute calibration uncertainty, whichever is larger.

extending to the E and NE apparently overlapping H79f. Our new 21cm observations cover a wider velocity range (4275–4880 km s^{-1}) with detections in the range 4470–4680 km s^{-1} (see Figure 18). While most of the emission originates in H79d, the new observations (see Figure 17) clarify the structure of the H I tail towards the east. We do not confirm an overlap with H79f and find all the eastward emission to be south of that galaxy. The velocities for the eastward emission are continuous with the emission from H79d. This is either a coincidence or evidence that we are seeing the first stages in the ISM stripping of H79d. The latter interpretation would exacerbate the problem of the missing gas in SS (Verdes-Montenegro et al. 2001) leaving no residual gas from galaxies H79a, b, c, or f.

The velocities in the eastern tidal tail are similar to the velocities in the southern part of galaxy H79d (see Figure 18—channel map at 4503 km s^{-1}). Long one-sided H I tails have been found in Virgo cluster spirals (Chung et al. 2007). Simulations of one of these galaxies, NGC 4654, suggests that ram-pressure stripping may be the cause of such H I tails (Vollmer 2003). These galaxies are interpreted as recent arrivals into the Virgo cluster (Chung et al. 2007). If this interpretation applies to H79d then the tail may be telling us that it entered the group from the NE. This does not provide additional support for the hypothesis that H79d is cross-fuelling H79a because the lowest velocity H I that falls near H79a shows a velocity $\sim 4550 \text{ km s}^{-1}$

(see Figure 18) which is $\sim 200 \text{ km s}^{-1}$ higher than the infalling gas.

Verdes-Montenegro et al. (2001) argued that SS as a group was very deficient in cold gas, traced by H I emission. They estimated the H I deficiency in the range of 30–50% depending on whether one assumes that HCG79bc are intrinsically S0 galaxies or were originally spirals. Similar numbers were obtained for SQ. The most extreme estimates are motivated by the possibility that all E and S0 galaxies in CG are the product of spiral galaxy “harassment” (disk destruction and ISM stripping) as proposed to explain the S0 population in galaxy clusters (Moore et al. 1996). This assumption is further supported by the very high fraction (~ 80 – 85%) of late-type galaxies found in low-density environments (Sulentic et al. 2006) which we argue are typical of CG environments. If we assumed that H79a and f were also originally spirals then we would obtain an even more extreme deficiency ($\sim 70\%$). Velocity ranges sampled by old and new 21cm observations of SS unfortunately do not include the full range of possible velocities implied by optical measures. It is reasonable to expect H I with velocities as low as $\sim 4000 \text{ km s}^{-1}$. The mean velocity of galaxy H79c is close to 4000 km s^{-1} , so stripped gas might reasonably be expected down to $\sim 3800 \text{ km s}^{-1}$. Comparison of the new VLA H I spectrum with single-dish Arecibo (Biermann et al. 1979; Gallagher et al. 1981) and GBT (Borthakur et al., in preparation) H I velocity

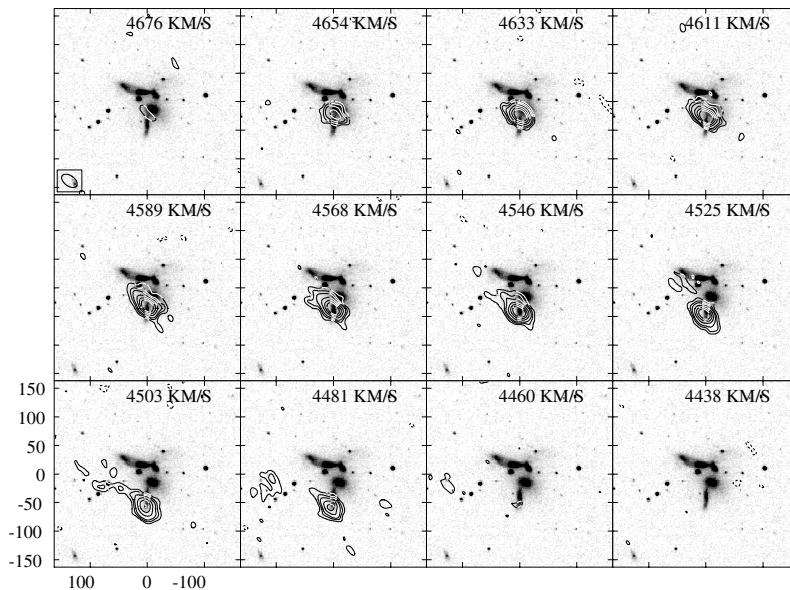


Figure 18. VLA: H I channel maps.

profiles suggest extended emission ($\sim 20\%$ of total) might exist between $3900\text{--}4800\text{ km s}^{-1}$. An unpublished position–velocity plot that includes the region north of H79d shows evidence for another H I component beginning at 4250 km s^{-1} near the edge of our velocity range. We suggest a conservative estimate of 30% H I deficiency for both SQ and SS.

The observed H I mass of galaxy H79d agrees with the mass predicted for its blue luminosity (Verdes-Montenegro et al. 2001). On the other hand, the H I mass for H79d is lower than the mean value for Sd galaxies (Roberts & Haynes 1994). The position–velocity (PV) plot for H79d (Figure 19) shows an almost solid-body rotation curve as expected for a low mass disk galaxy. One can see four fairly equally spaced peaks in the PV plot, which likely correspond to spiral arms in the disk. The corresponding local peaks can be seen in the H α image as well (see Figures 8 and 9).

No molecular gas has been detected in SS although, again, only part of the plausible velocity range has been sampled. H₂ masses traced by CO emission have upper limits of $\sim 5 \times 10^8 M_{\odot}$, $6 \times 10^8 M_{\odot}$, $6 \times 10^8 M_{\odot}$ for H79a,b and c, respectively (Leon et al. 1998; Verdes-Montenegro et al. 1998).

3.7. X-Ray

While the general process producing H I deficiency in a large number of CG is yet to be clarified, their results suggest that gas heating may play a role and that very sensitive X-ray maps and flux measurements could be a way to look for hot gas. In the case of SS the soft X-ray emission has an upper limit of $L_X < 2.3 \times 10^{41}\text{ erg s}^{-1}$ (Ponman et al. 1996), using ROSAT PSPC (position sensitive proportional counter) data. According to Pildis et al. (1995a), using the same data, this estimate is a 2.6σ detection. Thus, there is no massive soft X-ray emitting halo of hot gas. This might indicate a dynamical old system where gas has cooled. On the other hand, N2000a have argued that the 2.6σ photon excess in SS is consistent with an extended halo component that follows the diffuse optical light.

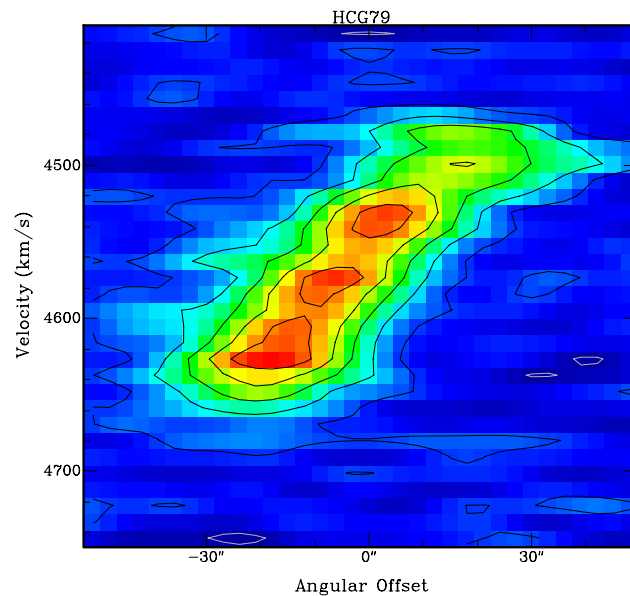


Figure 19. VLA: H I position–velocity plot of H79d along major axis (PA = 180°).

(A color version of this figure is available in the online journal)

4. DISCUSSION

We report multiwavelength observations of SS that seek to explore the evolutionary history of the group especially in the context of previous work on SQ. We assume SS and SQ are representative of the CG phenomenon (H1982; Sulentic 1997) and that SS is considerably more evolved than SQ. The first assumption is based on the fact that both groups show $n = 4$ or more accordant redshift members with evidence that virtually all are interacting. The second assumption is based upon the much higher luminosity fraction contained in the SS halo (Section 3.1.3). SQ is unusual at this time because a new intruder is entering the group at unusually high velocity. Our inferences

about SQ as a typical CG were only marginally affected by this transient event. That collision is generating excess X-ray, optical emission line and radio radiation. The closest equivalent in the southern CG sample (Iovino 2002) would likely involve the “Cartwheel” system where we are observing the aftermath of a disk-penetrating collision. The frequency of occurrence of such spectacular events depends upon (1) the density of high-velocity neighbors near CGs and/or (2) the number of groups with high enough mass concentration capable of accelerating neighbors into a group with suitably high velocity. Most CGs are not found in regions of high enough density for high velocity $\Delta V \sim 10^3 \text{ km s}^{-1}$ intruders to be common. Yet SQ is certainly not the only group with such a potential intruder (see Figure 2 in Sulentic 1997). The important point to emphasize is that groups like SQ that are currently undergoing a spectacular event are no less typical because of it.

Specific considerations involve (1) the age of the group, (2) the nature of its tidally truncated members, (3) the nature and origin of its luminous halo, (4) the evidence for merger/accretion events, and, in view of its H I deficiency, (5) the fate of the missing gas. Compact groups can provide valuable insights into the role of extreme interactions on galaxy evolution and may be useful for interpreting results at higher redshift. It was once thought that unstable systems such as CGs had very short evolutionary lifetimes that ended in a merger catastrophe (e.g. Mamon 1987; Barnes 1989); however, observations do not support that view (Sulentic 1987, 1997), and hypothesized dark matter halos appear able to extend CG lifetimes indefinitely (e.g. Athanassoula et al. 1997).

SQ is the most studied compact group with published studies spanning the electromagnetic spectrum (Sulentic et al. 2001 and references therein plus subsequent), X-ray (Trinchieri et al. 2003, 2005), UV (Xanthopoulos et al. 2004; Xu et al. 2005), optical (Gutiérrez et al. 2002; Xu et al. 2003), MIR (Appleton et al. 2006), CO (Yun et al. 1997; Lisenfeld et al. 2002, 2004), H I (Williams et al. 2002), and radio continuum (Xu et al. 2003; Xanthopoulos et al. 2004) observations. If SQ can be viewed as a currently hyperactive prototype of the CG phenomenon, then we infer the following.

- (1) Compact groups form by slow sequential acquisition of neighbors from surrounding larger-scale structure. Nucleation points around which the process might begin could involve dark matter density fluctuations. Baryonic (primordial merger) fluctuations (Governato et al. 1996) are disfavored by the rarity ($\sim 10\%$) of first-ranked early-type galaxies in CGs (Sulentic 1997). Random continuous formation from more diffuse galaxy aggregates (e.g. Diaferio et al. 1994) is also disfavored for several reasons (see also Sulentic 1997): (a) local environmental densities are too low to make this process important, (b) few of the predicted majority population of transient groups are observed, and (c) observations indicate that compact group formation is slow and sequential.
- (2) New intruders are usually captured and quickly lose most of their ISM leading to (a) suppression of star formation within the galaxies, (b) possible stimulation of active nuclei due to infall of residual unstripped gas, and (c) morphological transformation from primarily spiral intruders into spiral bulges or into early-type E/S0 members. While brief episodes of enhanced star formation are expected and observed in CGs they are likely associated with the sequential arrival of new gas-rich intruders. This activity is unlikely to be long-lived if new arrivals are also rapidly stripped. SQ

suggests that any star formation activity that arises in the resultant debris field of stripped gas will be weak and will not approach the level expected from a single unstripped L^* spiral galaxy.

- (3) In addition to ISM stripping, which can create a multiphase gaseous debris field, the outer parts of the stellar components are stripped leading to the growth of a massive diffuse halo akin to what is now observed in some clusters. Some diffuse X-ray emission can be associated with this halo but this component is likely to be overestimated with low-resolution observations if (a) high-velocity intrusions take place, (b) AGN are common (e.g. HCG16), and (c) major mergers occur (yet rarely).
- (4) The major components of the groups persist as discrete (gas-poor early-type) condensations in a diffuse stellar halo for many Gyr. SQ is mute on the fate of these long-lived components but SS, viewed as a more evolved SQ, suggests that they may slowly dissolve into the hypergalactic halo before major merging can take place. The rarity of massive fossil ellipticals outside of cluster cores (Sulentic & Rabaça 1994) attests to the rarity of major mergers and the long timescale for the dissolution process. Groups such as SQ and SS disfavor hierarchical collapse scenarios.

Our new, as well as older published, measures for SS show many consistencies with what has been inferred from SQ. A complication in the case of SS may involve an unfavorable orientation where the principal plane of most components lies near edge-on to our line of sight. H79a, b, c, and d show morphological features, or axial ratios, consistent with the interpretation that they are highly inclined disk systems. Following the same numbering/lettering scheme above we evaluate the empirical clues available for SS. We refer to relevant subsections of Section 3 whenever our inferences are supported by particular observations or previously published work.

(1) *CG formation.* Galaxy H79d in SS is an example of the sequential acquisition process. Such acquisitions are likely to be rare given the low galaxy surface-density environment (Sulentic 1987; Rood & Williams 1989) in which SS is found. H79d could be regarded either as a simple projection along the same line of sight or as a galaxy that is entering the group for the first time. Yet, the low surface density of accordant and/or discordant galaxies near SS would justify the latter possibility. This highly inclined late-type (Sd) spiral shows H I (Section 3.6) and H α (Sections 3.2, 3.3) distributions consistent with the notion that all or most of the cold and warm ISM gas components are intact. New and old H α rotation curves (Section 3.3) also show little or no evidence for significant dynamical disruption. The slight “integral sign” shape of the galaxy can be argued to be the result of viewing a disk spiral at high inclination rather than the product of tidal deformation. H I emission extending towards NE (see Figure 17; see also Williams et al. 1991) could be interpreted as debris from earlier acquisitions although velocity continuity with the gas within H79d (Figure 18) makes this assumption uncertain, and can also be argued to be the beginning of the stripping process for that intruder. H α emission appears to link H79d with H79a (Figure 8; cross-fuelling?), although we do not find velocity continuity between emission on the side of H79d nearest H79a and the gas detected in its nuclear region (Section 3.3). We cannot unambiguously establish interaction of H79d with the rest of the group. Typical timescales for significant dynamical response and/or tidal stripping are $\sim 10^8$ years (Iono et al. 2004); this, coupled with the unequivocal evidence for lack of tidal perturbation suggests that, if

H79d is an intruder, it must have joined SS within this time frame.

H79c is the best candidate for the intrusion that preceded H79d into SS. It is the bluest (Section 3.1.4) member after H79d and also shows spectroscopic evidence (Section 3.3.2) for a reasonably young (~ 2 Gyr) stellar population perhaps generated just before it lost its ISM upon joining SS. H79f is the obvious candidate for the oldest, or one of the oldest, members of SS. It is sometimes described as a tidal tail (Nishiura et al. 2002), but its morphology (Section 3.1.2) and lack of a nonstellar component (Sections 3.2–3.6) are more consistent with the hypothesis that it is a remnant disk galaxy slowly dissolving into the common stellar halo (see also R1991, B1993, Bonfanti et al. 1999).

(2a) *H I stripping and SF suppression.* A statistical study of H I content in CG showed that H I deficiencies are common (Verdes-Montenegro et al. 2001). Both SQ and SS have estimated deficiencies in the range 30–70% depending on how many of the early-type components entered the groups as spirals (Section 3.6). All currently observed E and S0 components of SQ (3) and SS(4) are candidates because the environments that supply intruders are spiral rich. Two recently stripped spirals and, therefore, now proto-lenticulars (NGC7319 and 7320; Sulentic et al. 2001), can be identified in SQ. We suggest that H79d will likely suffer a similar fate. The reality of such gas deficiencies virtually guarantees a star formation deficit. FIR (Section 3.4) and $H\alpha$ (Section 3.2) observations are regarded as useful star formation diagnostics. Both are quite consistent with a normal (for its type and luminosity) level of star formation H79d. The lack of star formation suppression argues that it is the most recent SS intruder or a projected field galaxy. If H79d is viewed as a recent arrival into SS, this is apparently a much slower intrusion ($\Delta V \sim 200 \text{ km s}^{-1}$) than the ongoing one observed in SQ and is closer to the expectation for a low-velocity random capture in a low-density environment. A recent and low-velocity intrusion into SS can be also used to argue that no strong star formation enhancement would be expected at this time. In CG such disk starbursts are likely short-lived if rapid ISM stripping immediately follows the onset of the enhanced activity. Residual gas channeled into the nuclei of galaxies might give rise to low-level star formation or AGN activity. Nuclear fuelling might be particularly efficient in CG because of the quasi-continuous nature of the tidal perturbations. The excess of compact nuclear radio sources (Menon & Hickson 1985) and low-luminosity AGN (Coziol et al. 2004) in CG members supports this suggestion.

Little additional emission related to star formation is observed in the obviously more evolved members of SS which reflects the observed deficit of gas in the group. Apart from H79d, SS shows a much more extreme level of star formation suppression than SQ which is consistent with it being older and more evolved. $H\alpha$ observations indicate low-level star formation is likely present in H79b, probably connected with an accretion event and H79a possibly connected with a feedback event (Section 3.3.1). Line emission from H79b shows a reasonably symmetric rotation curve and may originate entirely from the counter-rotating component. This is consistent with star formation in a recently accreted dwarf companion (Section 3.3.1), although quoted $[N II]/H\alpha$ ratios are close to those for H79a (N2000a; Coziol et al. 2004; see also Table 11) and lie between the H II and Seyfert domains in emission line diagnostic diagrams (Kewley et al. 2006). The extended $H\alpha$ rotation curve (Figure 12) argues strongly in favor of star formation in this galaxy.

H79a shows evidence for both nuclear and near-nuclear emission components. The $H\alpha$ image in Figure 8 and velocity decoupling (Figure 11) are consistent with the near-nuclear gas as a feedback event, possibly the result of cross-fueling of gas stripped from H79d. Our Fabry–Pérot measures (Section 3.3.1) support this interpretation because the extranuclear component is redshifted relative to the H79a nucleus by about 150 km s^{-1} , which is consistent with the extranuclear gas viewed as infalling onto the side of H79a closest (in projection) to H79d (Section 3.3.1). However, no evidence for velocity continuity is found (Section 3.3.1), and emission on the side of H79d closest to H79a shows a velocity $\sim 300 \text{ km s}^{-1}$ higher than that of the extranuclear emission feature (see Figures 10 and 11). The observations would require a discrete infall or fueling event rather than a continuous flow of gas from H79d to H79a. All emission line measures for the gas in H79a should be treated with caution because the two emission components are separated by only $\sim 3''$ (Section 3.2). This, as well as confusion in the literature between members of the group, explains the large scatter among redshifts quoted for this galaxy in NED.

Table 15 provides an interesting comparison of integrated optical, IR and radio properties for SQ and SS along with corresponding data for the well-studied $L \sim L^*$ Sb spiral NGC7331. This provides an alternative demonstration of the H I and star formation deficits. SQ is \sim two integrated B magnitudes brighter than NGC7331, while SS shows approximately the same value as that galaxy, but with half of the luminosity in a diffuse halo (Section 3.1.3). SQ contains the same mass of H I as NGC7331 although it originally contained, at least, three spirals with similar luminosity to that galaxy. SS currently shows little more than the H I expected from a late-type spiral such as H79d (Verdes-Montenegro et al. 2001). Perhaps 20% more remains to be mapped using wider frequency coverage (Section 3.6). SQ and NGC7331 show similar integrated star formation measures. However, this is an overestimate of star formation activity in SQ because $H\alpha$ (via enhanced $[N II]$) and radio continuum emission in SQ are boosted by a large-scale shock (Moles et al. 1997; Sulentic et al. 2001), while those measures and FIR luminosity are boosted by the luminous AGN NGC7319. SS shows much lower levels of activity in all measures with H79d contributing most of the H I and about 60% of the $H\alpha$ emission (Section 3.2). While composed of less luminous galaxies, if formed from a largely spiral field, then SS represents an extreme example of star formation suppression. SQ is clearly evolving in that direction.

Another way to characterize the star formation suppression involves comparison of integrated colors and/or population synthesis measures for CG members. Our color measures (Section 3.1.4) indicate a dominance of older populations in H79abf and c (with a more recent component with age ~ 2 Gyr; Section 3.3.2). Other recent spectroscopic synthesis studies (de la Rosa et al. 2007; Proctor et al. 2004) suggest systematically older populations (compared to field galaxies) in larger samples of CG members. An earlier photometric study of elliptical members in CGs showed typical red colors and little or no evidence for a recent merger population (Zepf et al. 1991; Zepf 1993).

$H\alpha$ surveys of CG members (Vílchez & Iglesias-Páramo 1998; Iglesias-Páramo & Vílchez 1999) reveal a wide range of inferred star formation activity. Taken galaxy by galaxy, this is unsurprising. However, galaxies in the most evolved CGs (like SS) will show very low levels of star formation activity in most members except for the occasional unstripped

Table 15
Basic Properties for SS, SQ and NGC 7331

Name	$\log M_{\text{HbbxI}}$ (M_{\odot})	$\log L_{\text{H}\alpha}$ (L_{\odot})	$\log L_{\text{FIR}}$ (L_{\odot})	$\log L_B$ (L_{\odot})	M_B	$\log L_{1.4\text{ GHz}}$ (L_{\odot})
HCG 79	9.3 ^a	6.6 ^c	9.9 ^e	10.3 ^g	-21.0 ^g	4.3 ⁱ
HCG 92	10.0 ^a	7.4 ^d	10.2 ^e	11.2 ^g	-23.2 ^g	5.7 ^j
NGC 7331	10.0 ^b	7.8 ^b	10.3 ^f	10.5 ^h	-21.5 ^h	4.5 ^j

Notes. Column 1: galaxy/group identification. Column 2: logarithm of the H I mass. Column 3: logarithm of the H α luminosity. Column 4: logarithm of FIR luminosity. Column 5: logarithm of the total blue luminosity. Column 6: total blue absolute magnitude. Column 7: logarithm of 1.4 GHz radio continuum luminosity.

References. ^a Verdes-Montenegro et al. (2001); ^b Kennicutt Jr. & Charles (1994); ^c Coziol et al. (2004); ^d Severgnini et al. (1999); ^e Verdes-Montenegro et al. (1998); ^f Sanders et al. (2003); ^g Hickson (1993b); ^h RC3; ⁱ our VLA data; ^j NVSS.

new intruder. These inferences will be confused if triplets are included in a CG sample. Less evidence of dynamical evolution is expected in these more intrinsically unstable configurations. This is especially true for the most studied samples such as Hickson compact groups (HCGs) where hierarchical systems are rare.

(2b) *AGN.* Gas that is not stripped from CG members will likely suffer angular momentum dissipation leading to efficient channeling into component nuclei. There is accumulating evidence that galaxies in CGs show a higher frequency of, generally low level, AGN activity (Coziol et al. 2004; Martínez et al. 2006). This activity can take at least three forms: Seyfert, LINER, and H II nuclei, the last not really AGN in the classical sense although they have been argued to be a precursor to Seyfert activity (e.g. Barth & Shields 2000). Recently stripped NGC7319 in SQ hosts a luminous Seyfert 2 nucleus that is a strong source from radio to X-ray wavelengths. Both H79 a and b show evidence for nuclear activity at radio (Section 3.5), MIR (Section 3.4), and optical (Section 3.1) wavelengths. All H α emission outside of H79d is found near the centers of these two galaxies. Line ratios in H79a ([N II]/H α and [O III]/H β) (N2000a; Coziol et al. 2004) are consistent with LINER activity, according to the emission line diagnostic diagrams of Kewley et al. (2006), if the derived ratios involve the nuclear gas. Emission from H79b (NGC6027, VII Zw631) shows well-defined counter-rotation in the emission component (Section 3.3.1), and is likely dominated by star-forming gas in an accreted neighbor perhaps coupled with some weakly shocked gas. Radio continuum emission from H79a involves a point source at all VLA resolutions while H79b shows weaker and more extended emission (Section 3.5) which supports our inference that only H79a hosts an AGN at this time. Unless CG members host unusually low mass black holes, the weakness of most AGN activity must be due to low accretion rates where only residual gas remains to fuel nuclei. In systems where there is a quasi-continuous perturbation there is perhaps less opportunity to build up a reservoir of gas that episodically might fuel more intense AGN activity. The CG alternative might well involve longer phases of low-level activity.

(2c) *Morphological transformation.* SQ contains two recently stripped spirals and another spiral intruder in the process of being stripped (Sulentic et al. 2001). The remaining two members in SQ are either elliptical galaxies or remnant bulges of spirals. SS galaxies H79a, b, c, and f show early-type (albeit peculiar) morphologies (Section 3.1.2). In analogy with SQ we argue that most of these galaxies entered SS as spirals because the environment of SS is spiral rich (Section 3.1.1); they were

subsequently stripped and transformed into E/S0 systems. In the case of SQ some of the stripping events must have taken place recently because we can still recognize spiral structure (NGC 7319 and NGC7320c; Sulentic et al. 2001) while in SS the disks and associated spiral structure have been largely destroyed leaving remnant bulges imbedded in a stellar halo partly or mostly composed of the stripped disks. We also argue that the galaxies were considerably more luminous when they first entered SS. This is self-evident because the massive halo must have formed from stars that originated in existing and/or now disrupted members. The fraction of early-type members in SS (~ 0.7 – 0.8) is larger than expected if SS was formed from random infall of galaxies from its environment. The observed early-type fraction in the SS environment is ~ 0.3 – 0.4 (Section 3.1.2) above the expectation from the low-density environment of extremely isolated galaxies ~ 0.14 (Sulentic et al. 2006).

All known accordant redshift neighbors around SS are larger and brighter than members of the group (Sections 3.1.2, 3.1.3). Of course, the tabulation is likely biased towards the brightest members in the neighborhood if for no other reason than we are tabulating neighbors with measured redshift. All members of SS are smaller and most are fainter than this neighboring population. Taken at face value SS is a compact group of sub- L^* galaxies. Few tabulated compact groups of dwarf galaxies have been observed (Hickson et al. 1992; Iovino 2002), and there may be dynamical stability and hierarchical structural reasons for the paucity of dwarf compact groups. The four brightest accordant members of most tabulated groups tend to show similar $L \geq L^*$ luminosities (i.e. they are not hierarchical systems). Thus we argue that SS was formed by sequential accretion of luminous spiral galaxies that have undergone (1) gas stripping that transformed them into E/S0 morphologies, and (2) stellar stripping that has significantly reduced their sizes. This stellar harassment process might be similar to, but even more efficient than (because of lower systemic velocity dispersions), the one proposed to explain the existence of S0 galaxies in clusters (Moore et al. 1996). In CGs a significant population of spiral bulges may exist as “early-type” members.

The early-type members of SS are too bright for their size and this can be explained if disks are stripped leaving the higher M/L bulge region of each galaxy relatively intact. Comparison of the size and brightness of bulges in some of the bright neighboring spirals indeed shows values similar to those measured for the early-type members of SS (Section 3.1.3). The early-type members of SS are embedded in a relatively blue massive stellar halo (Section 3.1.3, 3.1.4). It is reasonable to assume that this

luminous halo was generated by stripping/dissipation processes involving the existing member galaxies. The relatively blue color of the halo supports the idea that much of it came from a disk stellar population. The excess brightness for their size (i.e. compactness) of SS members will also be abetted by minor accretion events of the kind that we observe in H79b.

If most SS members began as spiral intruders, then we are faced with a serious deficit of stripped hot/warm/cold gas in and around SS (Sections 3.2–3.7; see also Verdes-Montenegro et al. 2001). In the case of SQ we found all three components in the intergalactic medium (IGM) although little was found within the group members. Part of the H I deficit in SQ is now shocked to X-ray-emitting temperatures (Trinchieri et al. 2003, 2005) some of which may have cooled and condensed into H II regions (Xu et al. 1999; Sulentic et al. 2001). In SS we observe only $\log M_{\text{H I}}(M_{\odot}) = 9.3$ (Verdes-Montenegro et al. 2001) most of which is concentrated in H79d.

The existence of “passive spirals” (Goto et al. 2003b) could possibly help solve the problem of “missing gas” (gas deficit) in CGs. For example, one could envision a scenario in which the members of SS entered the group as extremely gas-poor spiral galaxies. As Goto et al. (2003b) suggests, such galaxies seem to prefer environment density $\sim 1\text{--}2 \text{ Mpc}^{-2}$, similar to the SS neighborhood (Section 3.1.1). On the other hand, these gas-deficient spiral galaxies are very rare ($\sim 0.28\%$, i.e. they found 73 cases from a sample of 25,813) and quite red (almost as red as elliptical galaxies). The members of SS seem to be bluer (see our Table 9) than those “passive spirals” (see Figure 9 in Goto et al. 2003b). A search (dedicated study) for potential “passive spirals” among the neighbors of CGs merits further attention.

Compact groups pose a problem for radio line (and often Fabry–Pérot) studies because the velocity range over which gas might be present can be large. In the case of SQ, optical emission and absorption line velocities span almost 2000 km s^{-1} (1200 km s^{-1} in detected H I). Optical velocities in SS span a range close to 700 km s^{-1} with at least two condensations in H I at $4400\text{--}4700 \text{ km s}^{-1}$ (H79d and tail towards E) and $\sim 4200 \text{ km s}^{-1}$ possibly associated with H79a and not well defined in our new or in previous observations (Section 3.6). Earlier single dish measures (Biermann et al. 1979; Gallagher et al. 1981; Gordon & Gottesman 1981) already raised the possibility of H I at velocities both higher and lower than H79d. We confirm the latter, but given the scatter among previous single-dish mass estimates it is difficult to estimate how much H I we may have missed. We cannot rule out the possibility that significant H I stripped more than 1.5 Gyr ago remains undetected. This is required in assuming that most of the galaxies H79abcf entered SS as spirals. A conservative estimate for the total H I content within SS ($\log M_{\text{H I}}(M_{\odot}) \sim 9.4\text{--}9.5$) is based on the single-dish H I measures. The same comments apply to previous searches for molecular gas in SS (Leon et al. 1998; Verdes-Montenegro et al. 1998). At the other extreme only a small hot X-ray-emitting component was detected by ROSAT (Section 3.7) which may be associated with the diffuse stellar halo (N2000a).

Either our assumption that SS was formed from spirals is incorrect or we must account for considerable (30–70%) missing gas (Section 3.6). We have no evidence for extreme starbursts in less-evolved compact groups that should be viewed as the precursors of an SS system. In fact, as dynamically hyperactive systems CGs are surprisingly deficient in FIR emission (e.g. Verdes-Montenegro et al. 1998). Thus gas depletion via star

formation seems unlikely to explain such a large deficit. Both H I/CO mapping of a wider spatial/velocity field and deeper searches for a warm gas component (OSIRIS-GTC?) might yield interesting results.

(3) *Diffuse halo formation.* After an initial period of negative results (Rose 1977; Sulentic & Lorre 1983; Pildis et al. 1995b) luminous optical halos have now been found in many CGs (D2005 Sulentic 1987; Pildis et al. 1995b; Sulentic 1997; White et al. 2003; Aguerri et al. 2006). Estimated diffuse light fractions range from a few percent up to 50%, suggesting that this measure might be a useful diagnostic for the dynamical age of a CG. Recent studies of the SQ halo show it to be very complex with an integrated luminosity of $\sim L^*$ (\sim average luminosity of one L^* galaxy) (Moles et al. 1998) and therefore representing about 20% of the total group luminosity. A more sensitive study (Gutiérrez et al. 2002) suggests that 20% might be underestimated. *VR/I* measures (N2000a) yielded an estimate of 12–13% for the halo in SS. More recent wavelet processing of deep CCD images (D2005) suggests that the halo luminosity fraction is $\sim 46\%$ in the *B* band which agrees with our own estimate (Section 3.1.3). We reduce the D2005 estimate to 40% because we cannot confirm an apparent extension towards the east which, we suggest, may be an artifact induced by some relatively bright stars about one group diameter in that direction (see Figure 6 in D2005). We conclude that the halo fraction in SS is approximately twice that in SQ. On this basis alone we conclude that SS is a much older group than SQ.

Sommer-Larsen (2006) studied the diffuse light in “fossil” groups (FGs) (e.g., hierarchical groups with a very bright central galaxy) and non-fossil groups (non-FGs) (e.g., groups with galaxies of similar brightness, i.e. non-hierarchical). Their models predict halo contributions of $\sim 12\text{--}45\%$ with a higher fraction of diffuse light in FGs. Most CGs (up to 90%) tend to be non-hierarchical which is a long-standing argument against a major merger evolutionary scenario to account for them (Sulentic 1997; see also Proctor et al. 2004; de la Rosa et al. 2007 for a different form of evidence). SQ and SS are certainly non-hierarchical configurations with halo fractions that appear to exceed the above model expectations. SS provides the strongest challenges to formation models with a very massive halo that is also somewhat bluer than the galaxies embedded within it (see Table 9). It points towards a slow sequential “dissolution” process without significant major merger activity. Additional support for this conclusion comes from the fact that highly evolved SS is a very weak X-ray emitter compared to many detected compact and loose groups (Helsdon & Ponman 2000) with estimates for any soft halo component near $L_X \sim 10^{40} \text{ erg s}^{-1}$ (N2000a). Before dismissing SS as atypical it is worth pointing out that the X-ray luminosity of SQ is strongly boosted by a transient shock component (Trinchieri et al. 2005). The X-ray weak halo component in SQ (Helsdon & Ponman 2000) appears to be about 1 dex higher than any equivalent component in SS.

(4) *Long-lived system.* We earlier estimated a minimum age for SQ of 2–3 Gyr based upon encounter events that we could identify over the past 1–2 Gyr (Sulentic et al. 2001). Various studies have identified a sequence of compact group ages, or evolutionary stages, using H I morphology/deficiency (Verdes-Montenegro et al. 2001), diffuse light fraction (Aguerre et al. 2006), and dynamical inferences (Ribeiro et al. 1998). The fraction of early-type galaxies normalized by local environmental density (Goto et al. 2003a) offers an additional measure (Section 3.1.2). All measures suggest that SQ is reasonably evolved and

that SS is significantly more evolved than SQ. If we assume that the halo age is directly proportional to the luminosity fraction, then we can assume a minimum age for SS of 4–6 Gyr. The episodic accretion rate in SS appears to be slower than for SQ and this will slow down the evolutionary process. If nothing precludes compact group formation in richer environments one expect many to form but with a large fraction that are transient (e.g. Diaferio et al. 1994, 1995). No more than 10% of HCG fall in this category (Sulentic 1987; Rood & Williams 1989). This would not be the slow sequential process that characterizes SQ and SS.

In the case of SS one could identify H79d as the most recent arrival while H79c likely arrived more than 1.5 Gyr ago. Both the new intruder and the accreted object in H79b are relatively low-mass galaxies (Section 3.3.1). Our optical and H α reconnaissance of the SS neighborhood reveals no other prospective intruders for the next \sim 5 Gyr (Section 3.1.1). Apparently after acquiring the nearest 4–5 neighbors a “typical” CG (in lower-density environments) such as SQ or SS creates a local void after which it very rarely acquires additional members.

A possible new way to estimate dynamical ages in CGs is provided by the *HST* search for young blue star clusters (BSCs) thought to form via interactions. A large number of candidate BSCs have been identified in SQ (Gallagher et al. 2001) although their true nature remains unconfirmed. A contradiction is provided by the almost total absence of BSC candidates in SS (Palma et al. 2002) which at 2/3 the distance should have been easier to detect. Numerous red star cluster candidates were found around SS galaxies. Our own high-pass filtering of archival WFPC images of H79a appears to show a halo of assumed globular clusters surrounding that galaxy. If we assume that the condensations in SQ are BSCs and that they are a signature of major accretion/interaction events, then SQ has undergone significant activity in the past Gyr which is well confirmed by numerous observations (and more recent references cited earlier; Sulentic et al. 2001). *HST* imaging analysis shows the candidate star cluster color distributions for SQ peak at $B - V \sim 0.1$ and $V - I \sim 0.4$ (Gallagher et al. 2001) while corresponding average colors in SS are $B - V \sim 0.5$ and $V - I \sim 1.0$ (Palma et al. 2002). This suggests no SS star cluster population with an age of less than 1 Gyr, roughly consistent with our suggestion that H79c was the last major intruder about 2 Gyr ago. We interpret galaxies H79abcf as old arrivals and this is supported by the degree of tidal stripping evidenced through their surface photometric properties and the luminosity fraction in the halo. Any BSCs associated with these past intrusions have now become significantly redder.

Galaxies H79abcf are assumed to be the stripped cores of old spiral intruders. The somewhat bluer color of the diffuse light (Section 3.1.4, D2005) is then consistent with the hypothesis that much of the halo mass came from stripped spiral disks. This bluer halo color is also evidence that SS formed long ago from a largely spiral population that has been strongly secularly evolved. Galaxy H79f is interpreted as the most extreme example of this process. It has been extensively studied (Nishiura et al. 2002) and has been interpreted both as a tidal feature (Nishiura et al. 2002) and as the remnant of a disrupted galaxy (Bonfanti et al. 1999). The central brightness concentration and concentric luminosity isophotes about the center of this feature argue for the second interpretation. We suggest that this is the most evolved member of the group and offers an empirical insight into the dynamical evolution of

compact group members via dissolution rather than merging. The more remnant cores we identify in SS, the lower the average initial luminosity of the intruders. If lower-luminosity spirals have a higher average gas fraction then inclusion of H79f as an intruder remnant actually exacerbates the H I deficit.

We used rotation curves (H79bd) and velocity dispersion measures (H79a) to estimate masses for different components of SS (Section 3.3.1). Masses for H79c and f are estimated via an assumed M/L ratio ~ 10 (Bacon et al. 1985). Galaxies H79b, c, and d are each estimated to be $\sim 10^{10} M_{\odot}$ with H79a $\sim 5 \times 10^{10} M_{\odot}$ and H79f $\sim 5 \times 10^9 M_{\odot}$. We must add almost $10^{10} M_{\odot}$ for the H I mass. Given truncated luminosity estimates for the galaxies and perturbed or truncated rotation curves these values are likely underestimates. The total mass of discrete components probably lies in the range of $10^{11} M_{\odot}$ which is similar to our estimate for the halo mass. While likely not as massive as SQ, SS was not formed from a dwarf population although most of the members may have entered as slightly sub- L^* galaxies.

The lack of major mergers and first-ranked ellipticals in compact groups (Mendes de Oliveira & Hickson 1991; Sulentic & Rabaça 1994) as well as the rarity of fossil ellipticals in low-density galaxy environments (Sulentic & Rabaça 1994; Zabludoff & Mulchaey 1998) make clear that such groups evolve very slowly and likely require massive DM halos (Athanasoula et al. 1997; Aceves & Velázquez 2002). Thus hierarchical collapse models (Baugh et al. 1996; Kauffmann 1996; Kauffmann & Charlot 1998) are strongly disfavored. SQ and SS further support these conclusions with no evidence for major mergers. In one sense there is agreement star formation is rapidly quenched/truncated in CGs (de la Rosa et al. 2007). This appears to contradict predictions of monolithic collapse models (Chiosi & Carraro 2002) where star formation continues for a much longer time. It is important to point out that none of these models makes predictions about structure at such high spatial frequencies as typified by SQ and SS. SS offers one striking example of a minor merger while none has been identified in SQ.

If the majority of SS members are correctly interpreted as cores of stripped spiral then it is clear that this group, and perhaps most groups, dynamically evolve via dissolution rather than major mergers. Rather than the “beginning of the end” (Palma et al. 2002) SS is engaged in a slow process that has already persisted for a significant fraction of Hubble time. If (1) fossil ellipticals are rare (Mulchaey & Zabludoff 1999; Sulentic & Rabaça 1994), and, concomitantly, (2) major mergers in CGs are rare (Sulentic 1997), and (3) groups with more than five members are rare, then we are forced to conclude—without resorting to magic dark substances—that most CGs such as SQ and SS that ever formed are still in existence.

One of us (A.D.) acknowledges support from a Graduate Council Research/Creative Fellowship offered by the Graduate School of the University of Alabama for the 2006/2007 academic year. A.D. also thanks R.J. Buta and W.C. Keel for helpful discussions. M.R. acknowledges grants 46054-F from CONACYT and IN100606 from DGAPA-UNAM, Mexico. A.d.O. and J.P. are partially supported by Spanish research projects AYA2006-1325, AYA2006-1213 and Junta de Andalucía TIC114. We thank C. Da Rocha for providing the CFHT images of the diffuse light component in SS. We acknowledge V. Avila-Reese for helpful comments. We also acknowledge P. Amram and C. Balkowski for making the run to obtain the CFHT H α

F-P images. The new radio data presented in this paper were obtained with the NRAO instrument, the VLA. A.I. acknowledges financial contribution from the contract ASI-INAF I/023/05/0.

REFERENCES

- Aceves, H., & Velázquez, H. 2002, *Rev. Mexicana Astron. Astrofis.*, **38**, 199
- Adelman-McCarthy, J. K., et al. 2007, [arXiv:0707.3380](https://arxiv.org/abs/0707.3380)
- Aguerri, J. A. L., et al. 2006, *A&A*, **457**, 771
- Allam, S., et al. 1996, *A&AS*, **117**, 39
- Amram, P., Boulesteix, J., Georgelin, Y. M., Laval, A., Le Coarer, E., Marcelin, M., & Rosado, M. 1991, *ESO Messenger* (ISSN 0722-6691), no. 64, p. 44
- Amram, P., Le Coarer, E., Marcelin, M., Balkowski, C., Sullivan, W. T. III, & Cayatte, V. 1992, *A&AS*, **94**, 175
- Appleton, P. N., et al. 2006, *ApJ*, **639**, L51
- Athanassoula, L., Makino, J., & Bosma, A. 1997, *MNRAS*, **286**, 825
- Bacon, R., Monnet, G., & Simien, F. 1985, *A&A*, **152**, 315
- Barnby, P., & Huchra, J. P. 1998, *AJ*, **115**, 6
- Barnes, J. E. 1989, *Nature*, **338**, 123
- Barth, A. J., & Shields, J. C. 2000, *PASP*, **112**, 753
- Baugh, C. M., Cole, S., & Frenk, C. S. 1996, *MNRAS*, **283**, 1361
- Beers, T. C., et al. 1995, *AJ*, **109**, 874
- Bender, R., Burstein, D., & Faber, S. M. 1992, *ApJ*, **399**, 462
- Bettoni, D., & Fasano, G. 1993, *AJ*, **105**, 1291 (B1993)
- Biermann, P., Clarke, J. N., & Fricke, K. J. 1979, *A&A*, **75**, 19
- Biviano, A. 1998, The ISOCAM Calibration Error Budget Report, ver. 3.1
- Bonfanti, P., Simien, F., Rampazzo, R., & Prugniel, Ph. 1999, *A&AS*, **139**, 483
- Boulesteix, J. 1993, Manual of the ADHOC software
- Bruzual, G., & Charlot, S. 2003, *MNRAS*, **344**, 1000
- Burstein, D., & Heiles, C. 1982, *AJ*, **87**, 1165
- Carnevali, P., Cavaliere, A., & Santangelo, P. 1981, *ApJ*, **249**, 449
- Cesarsky, C. J., et al. 1996, *A&A*, **315**, 32
- Chiosi, C., & Carraro, G. 2002, *MNRAS*, **335**, 335
- Chung, A., van Gorkom, J. H., Kenney, J. D. P., & Vollmer, B. 2007, *ApJ*, **659**, L115
- Condon, J. J., Anderson, M. L., & Helou, G. 1991, *ApJ*, **376**, 95
- Condon, J. J., Cotton, W. D., Greisen, E. W., Yin, Q. F., Perley, R. A., Taylor, G. B., & Broderick, J. J. 1998, *AJ*, **115**, 1693
- Coziol, R., Brinks, E., & Bravo-Alfaro, H. 2004, *AJ*, **128**, 68
- Da Rocha, C., & Mendes de Oliveira, C. 2005, *MNRAS*, **364**, 1069 (D2005)
- de la Rosa, I. G., de Carvalho, R. R., & Zepf, S. E. 2001, *AJ*, **122**, 93
- de la Rosa, I. G., de Carvalho, R. R., Vazdekis, A., & Barbuy, B. 2007, *AJ*, **133**, 330
- de Carvalho, R. R., Ribeiro, A. L. B., Capelato, H. V., & Zepf, S. E. 1997, *ApJS*, **110**, 1
- de Vaucouleurs, G., et al. 1991, Third Reference Catalog of Bright Galaxies (New York: Springer), 110, (RC3)
- Diaferio, A., Geller, M. J., & Ramella, M. 1994, *AJ*, **107**, 868
- Diaferio, A., Geller, M. J., & Ramella, M. 1995, *AJ*, **109**, 2293
- Dickel, J. R., Rood, H. J., & Williams, B. A. 1984, ed. F. Mardirossian, G. Giuricin, & M. Mezzetti Clusters and Groups of Galaxies (Boston, MA: Reidel), 109, 389
- Dickey, J. M., & Salpeter, E. E. 1984, *ApJ*, **284**, 461
- Faber, S. M., & Jackson, R. E. 1976, *ApJ*, **204**, 668
- Falco, E. E., et al. 1999, *PASP*, **111**, 438
- Fitzpatrick, E. L. 1999, *PASP*, **111**, 63
- Freudling, W. 1995, *A&AS*, **112**, 429
- Fuentes-Carrera, I., et al. 2004, *A&A*, **415**, 451
- Gallagher, J. S., Knapp, G. R., & Faber, S. M. 1981, *AJ*, **86**, 1781
- Gallagher, S. C., et al. 2001, *AJ*, **122**, 163
- García, A. M. 1993, *A&AS*, **100**, 47
- González Delgado, R. M., Cerviño, M., Martins, L. P., Leitherer, C., & Hauschildt, P. H. 2005, *MNRAS*, **357**, 945
- Gordon, D., & Gottesman, S. T. 1981, *AJ*, **86**, 161
- Governato, F., Tozzi, P., & Cavaliere, A. 1996, *ApJ*, **458**, 18
- Goto, T., et al. 2003a, *MNRAS*, **346**, 601
- Goto, T., et al. 2003b, *PASJ*, **55**, 757
- Gruppioni, C., Pozzi, F., Zamorani, G., Ciliegi, P., Lari, C., Calabrese, E., La Franca, F., & Matute, I. 2003, *MNRAS*, **341**, 1
- Gutiérrez, C. M., López-Corredoira, M., Prada, F., & Eliche, M. C. 2002, *ApJ*, **579**, 592
- Helsdon, S. F., & Ponman, T. J. 2000, *MNRAS*, **319**, 933
- Helou, G., Khan, I. R., Malek, L., & Boehmer, L. 1988, *ApJS*, **68**, 151
- Hickson, P. 1982, *ApJ*, **255**, 382 (H1982)
- Hickson, P., Kindl, E., & Auman, J. 1989a, *ApJS*, **70**, 687 (H1989a)
- Hickson, P., Menon, T. K., Palumbo, G. G. C., & Persic, M. 1989b, *ApJ*, **341**, 679
- Hickson, P., Mendes de Oliveira, C., Huchra, J. P., & Palumbo, G. G. 1992, *ApJ*, **399**, 353
- Hickson, P. 1993a, *Astrophys. Lett.*, **29**, 1
- Hickson, P. 1993b, Atlas of Compact Groups of Galaxies (New York: Gordon and Breach Science Publishers)
- Hickson, P. 1997, *ARA&A*, **35**, 357
- Holtzman, J. A., et al. 1992, *AJ*, **103**, 691
- Iglesias-Páramo, J., & Vílchez, J. M. 1999, *ApJ*, **518**, 94
- Iono, D., Yun, M. S., & Mihos, J. C. 2004, *ApJ*, **616**, 199
- Iovino, A. 2002, *AJ*, **124**, 2471
- James, P. A., et al. 2004, *A&A*, **414**, 23
- Jester, S., et al. 2005, *AJ*, **130**, 873
- Kauffmann, G. 1996, *MNRAS*, **281**, 487
- Kauffmann, G., & Charlot, S. 1998, *MNRAS*, **294**, 705
- Kauffmann, G., et al. 2003, *MNRAS*, **341**, 33
- Keller, S. C., & Wood, P. R. 2006, *ApJ*, **642**, 834
- Kennicutt Jr., R. C. 1983, *ApJ*, **272**, 54
- Kennicutt Jr., R. C., Tamblyn, Peter, Congdon, & Charles, E. 1994, *ApJ*, **435**, 22
- Kennicutt Jr., R. C. 1998, *ARA&A*, **36**, 189
- Kent, S. M. 1985, *ApJS*, **59**, 115
- Kessler, M. F., et al. 1996, *A&A*, **315**, 27
- Kewley, L. J., Groves, B., Kauffmann, G., & Heckman, T. 2006, *MNRAS*, **372**, 961
- Köppen, J., & Arimoto, N. 1990, *A&A*, **240**, 22
- Kormendy, J., & Djorgovski, S. 1989, *ARA&A*, **27**, 235
- Landolt, A. U. 1983, *AJ*, **88**, 439
- Landolt, A. U. 1992, *AJ*, **104**, 340
- Laval, A., Boulesteix, J., Georgelin, Y. P., Georgelin, Y. M., & Marcelin, M. 1987, *A&A*, **175**, 199
- Le Coarer, E., et al. 1993, *A&A*, **280**, 365
- Leon, S., Combes, F., & Menon, T. K. 1998, *A&A*, **330**, 37
- Lisenfeld, U., et al. 2002, *A&A*, **394**, 823
- Lisenfeld, U., et al. 2004, *A&A*, **426**, 471
- Lisenfeld, U., et al. 2007, *A&A*, **462**, 507
- Macchetto, F., et al. 1996, *A&AS*, **120**, 463
- Mamon, G. A. 1987, *ApJ*, **321**, 622
- Martínez, M. A., del Olmo, A., Perea, J., & Coziol, R. 2006, ed. I. Saviane, V. Ivanov, & J. Borissova Groups of Galaxies in the Nearby Universe, in press (arXiv astro-ph/0611098)
- McCall, M. L. 2004, *AJ*, **128**, 2144
- Mendes de Oliveira, C., & Hickson, P. 1991, *ApJ*, **380**, 30
- Mendes de Oliveira, C., & Hickson, P. 1994, *ApJ*, **427**, 684
- Mendes de Oliveira, C., Amram, P., Plana, H., & Balkowski, C. 2003, *AJ*, **126**, 2635
- Menon, T. K., & Hickson, P. 1985, *ApJ*, **296**, 60
- Moles, M., Sulentic, J. W., & Marquez, I. 1997, *ApJ*, **485**, L69
- Moles, M., Marquez, I., & Sulentic, J. W. 1998, *A&A*, **334**, 473
- Moore, B., Katz, N., Lake, G., Dressler, A., & Oemler, A. 1996, *Nature*, **379**, 613
- Moshir, M., et al. 1990, IRAS Faint Source Catalogue, version 2.0
- Mulchaey, J. S., & Zabludoff, A. I. 1999, *ApJ*, **514**, 133
- Müller, K. R., et al. 1999, *A&AS*, **140**, 327
- Nishiura, S., et al. 2000a, *AJ*, **120**, 2355 (N2000a)
- Nishiura, S., et al. 2000b, *AJ*, **120**, 1691
- Nishiura, S., et al. 2002, *PASJ*, **54**, 21
- Osterbrock, D. E., & Ferland, G. J. 2006, Astrophysics of Gaseous Nebulae and Active Galactic Nuclei (2nd ed.; Sausalito, CA: University Science Books)
- Palma, C., et al. 2002, *AJ*, **124**, 2425
- Perea, J., del Olmo, A., Verdes-Montenegro, L., & Yun, M. S. 1997, *ApJ*, **490**, 166
- Phillips, M. M., et al. 1986, *AJ*, **91**, 1062
- Pildis, R. A., Bregman, J. N., & Evrard, A. E. 1995a, *ApJ*, **443**, 514
- Pildis, R. A., Bregman, J. N., & Schombert, J. M. 1995b, *AJ*, **110**, 1498
- Plana, H., et al. 2002, ed. M. Rosado, L. Binette, & L. Arias proceedings of Galaxies: The Third Dimension vol 282 (*ASP Conf. Ser.*), 282
- Ponman, T. J., Bourner, P. D. J., Ebeling, H., & Bohringer, H. 1996, *MNRAS*, **283**, 690
- Proctor, R. N., Forbes, D. A., Hau, G. K. T., Beasley, M. A., De Silva, G. M., Contreras, R., & Terlevich, A. I. 2004, *MNRAS*, **349**, 1381
- Ribas, I., et al. 2005, *ApJ*, **635**, L37
- Ribeiro, A. L. B., de Carvalho, R. R., Capelato, H. V., & Zepf, S. E. 1998, *ApJ*, **497**, 72
- Roberts, M. S., & Haynes, M. P. 1994, *ARA&A*, **32**, 115

- Rood, H., & Williams, B. 1989, *ApJ*, **339**, 772
- Rood, H. J., & Struble, M. F. 1994, *PASP*, **106**, 413
- Rosado, M., et al. 1995, *Rev. Mex. Astron. Astrofis. Ser. Conf.*, **3**, 263
- Rose, J. A. 1977, *ApJ*, **211**, 311
- Rubin, V. C., Hunter, D. A., & Ford Jr., W. K. 1991, *ApJS*, **76**, 153 (R1991)
- Salpeter, E. E. 1955, *ApJ*, **121**, 161
- Sanders, D. B., Mazzarella, J. M., Kim, D.-C., Surace, J. A., & Soifer, B. T. 2003, *AJ*, **126**, 1607
- Schlegel, D. J., Finkbeiner, D. P., & Davis, M. 1998, *ApJ*, **500**, 525
- Severgnini, P., Garilli, B., Saracco, P., & Chincarini, G. 1999, *A&AS*, **137**, 495
- Shimada, M., Ohyama, Y., Nishiura, S., Murayama, T., & Taniguchi, Y. 2000, *AJ*, **119**, 2664 (S2000)
- Siebenmorgen, R., Starck, J. L., Cesarsky, D. A., Guest, S., & Sauvage, M. 1996, *ISOCAM Data Users Manual*, SAI/95-222/Dc
- Sommer-Larsen, J. 2006, *MNRAS*, **369**, 958
- Stoughton, C., et al. 2002, *AJ*, **123**, 485
- Sulentic, J. W., & Lorre, J. J. 1983, *A&A*, **120**, 36
- Sulentic, J. W. 1987, *ApJ*, **322**, 605
- Sulentic, J. W., & de Mello Rabaça, D. F. 1993, *ApJ*, **410**, 520
- Sulentic, J. W., & Rabaça, C. 1994, *ApJ*, **429**, 531
- Sulentic, J. W., Rabaça, C. R., & Arp, H. 1994, ed. Isaac Shlosman proceedings of Mass-Transfer Induced Activity in Galaxies (Cambridge: Cambridge University Press), 429, 377
- Sulentic, J. W. 1997, *ApJ*, **482**, 640
- Sulentic, J. W., et al. 2001, *AJ*, **122**, 2993
- Sulentic, J. W., et al. 2006, *A&A*, **449**, 937
- Tarengi, M., Garilli, B., & Maccagni, D. 1994, *AJ*, **107**, 1629
- Tonry, J., & Davis, M. 1979, *AJ*, **84**, 1511
- Trinchieri, G., Sulentic, J., Breitschwerdt, D., & Pietsch, W. 2003, *A&A*, **401**, 173
- Trinchieri, G., Sulentic, J., Pietsch, W., & Breitschwerdt, D. 2005, *A&A*, **444**, 697
- Verdes-Montenegro, L., Yun, M. S., Perea, J., del Olmo, A., & Ho, P. T. P. 1998, *ApJ*, **497**, 89
- Verdes-Montenegro, L., et al. 2001, *A&A*, **377**, 812
- Vilchez, J. M., & Iglesias-Páramo, J. 1998, *ApJS*, **117**, 1
- Vollmer, B. 2003, *A&A*, **398**, 525
- White, P. M., Bothun, G., Guerrero, M. A., West, M. J., & Barkhouse, W. A. 2003, *ApJ*, **585**, 739
- Williams, B. A., McMahon, P. M., & van Gorkom, J. H. 1991, *AJ*, **101**, 1957
- Williams, B. A., Yun, M. S., & Verdes-Montenegro, L. 2002, *AJ*, **123**, 2417
- Xanthopoulos, E., Muxlow, T. W. B., Thomasson, P., & Garrington, S. T. 2004, *MNRAS*, **353**, 1117
- Xu, C., Sulentic, J. W., & Tuffs, R. 1999, *ApJ*, **512**, 178
- Xu, C. K., Lu, N., Condon, J. J., Dopita, M., & Tuffs, R. J. 2003, *ApJ*, **595**, 665
- Xu, C. K., et al. 2005, *ApJ*, **619**, L95
- Young, A. T. 1974, *ApJ*, **189**, 587
- Yun, M. S., Verdes-Montenegro, L., del Olmo, A., & Perea, J. 1997, *ApJ*, **475**, L21
- Zabludoff, A. I., & Mulchaey, J. S. 1998, *ApJ*, **496**, 39
- Zepf, S. E., Whitmore, B. C., & Levison, H. F. 1991, *ApJ*, **383**, 524
- Zepf, S. E. 1993, *ApJ*, **407**, 448